Journal of Materials Chemistry C

Nanostructured Copper Oxide Semiconductors: a Perspective on Materials, Synthesis methods and Applications

Journal:	*Journal of Materials Chemistry C*
Manuscript ID:	TC-FEA-02-2014-000345.R1
Article Type:	Feature Article
Date Submitted by the Author:	23-Apr-2014

Complete List of Authors:	Zoolfakar, Ahmad; RMIT University, School of Electrical and Computer Engineering; Universiti Teknologi MARA, Fakulti Kejuruteraan Elektrik Abdul Rani, Rozina; RMIT University, School of Electrical and Computer Engineering Morfa, Anthony J.; Freie Universität Berlin, Fachbereich Physik O'Mullane, Anthony; Queensland University of Technology, School of Chemistry, Physics and Mechanical Engineering Kalantar-Zadeh, Kourosh; RMIT University, School of Electrical and Computer Engineering

Journal of Materials Chemistry C RSCPublishing

REVIEW

Nanostructured Copper Oxide Semiconductors: a Perspective on Materials, Synthesis methods and Applications

Cite this: DOI: 10.1039/x0xx00000x

Received 00th January 2012,
Accepted 00th January 2012

DOI: 10.1039/x0xx00000x

www.rsc.org/

Ahmad Sabirin Zoolfakar,*[a,b] Rozina Abdul Rani[a], Anthony J. Morfa[c], Anthony P. O'Mullane[d] and Kourosh Kalantar-zadeh*[a]

The oxides of copper (Cu_xO) are fascinating materials due to their remarkable optical, electrical, thermal and magnetic properties. Nanostructuring of Cu_xO can further enhance the performance of this important functional material and provides it with unique properties that do not exist in its bulk form. Three distinctly different phases of Cu_xO, mainly CuO, Cu_2O and Cu_4O_3 can be prepared by numerous synthesis techniques including, vapour deposition and liquid phase chemical methods. In this article, we present a review of nanostructured Cu_xO focusing on their material properties, methods of synthesis and an overview of various applications that have been associated with nanostructured Cu_xO.

1. INTRODUCTION

Lately, there has been a great deal of interest in nanostructured copper oxide (Cu_xO) semiconductors. This interest in nanostructured Cu_xO is fuelled due to their remarkable physical and chemical properties as well as exciting prospects for a variety of applications.[1, 2]

Nanostructured Copper oxides are relatively abundant in nature[3], and a wide range of information is now available for their synthesis. Nanostructured Cu_xO can be grown using different synthesis techniques, including vapour and liquid phase deposition processes, in which a variety of nano morphologies can be obtained.

Nanostructured Copper oxides are exceptionally versatile and offer unique characteristics in many applications. Cu_xO nanomaterials have been used as colouring agents for the production of Roman mosaic glasses and antique ceramics for thousands of years.[4, 5] Nanosized Cu_xO has been widely utilized as a fungicids[6, 7] and in anti–fouling paints[8, 9] due to its biocide capability. With the advent of nanotechnology, Cu_xO has shown great impact in numerous research fields including optics, sensors, tribology, superconductor, electrochemistry and electronics.[10-14]

The most common crystal phases of Cu_xO are: (a) CuO also known as copper (II) oxide or cupric oxide where the mineral is known as tenorite, (b) Cu_2O also known as copper (I) oxide or cuprous oxide with the mineral name of cuprite, and (c) Cu_4O_3 with the mineral name of paramelaconite.[1, 2, 15, 16]

In this feature article, we present a general, yet complete, review of nanostructured Cu_xO. The present review is distinguishable from other reviews[1, 17], which have a focus on one type of Cu_xO (generally CuO or Cu_2O), while this review endeavor to thoroughly discuss three types of Cu_xO, including CuO, Cu_2O and Cu_4O_3. The organization of this review is as follows: firstly, we discuss the fundamental chemical and physical properties of nanostructured Cu_xO and then we summarize the different methods of synthesis that have been reported. Finally we present a selection of interesting applications that exploit Cu_xO and illustrate the enhancements made possible by using the nanostructured form of this material.

2. FUNDAMENTAL PROPERTIES

In this section, the fundamental properties such as crystal structures, electronic band structures, optical and electrical as well as transport properties of nanostructured Cu_xO are discussed. This section also describes the effect of doping or the presence of impurities on the properties of nanostructured Cu_xO.

2.1 Crystal Structure

CuO which has a black colour and crystallizes in monoclinic centered Bravais lattice in the space group of C2/c. The

crystallographic properties of CuO are tabulated in Table 1.[2, 15, 16, 18] The copper atom is coordinated to four coplanar oxygen atoms situated at the corners of a rectangular parallelogram, which form chains by sharing edges. The oxygen atom is coordinated to four copper atoms situated at the corners of a distorted tetrahedron. The chains traverse the structure in the [110] and [$\bar{1}$10] directions. The two types of chains alternate in the [001] direction and each type is stacked in the [010] direction with a separation between the chains of about 2.7 Å.[16, 18, 19]. Figure 1a demonstrates the crystal structure of CuO.

Cu_2O is the second stable phase of copper-oxide compounds which is reddish in colour. Cu_2O belongs to the cubic structure (space group, O_h^4 or $Pn\bar{3}m$) with a lattice constant of 4.2696 Å. Each Cu atom in the unit cell is coordinated by two oxygen atoms.[19] The crystallographic properties of CuO are tabulated in table 1. [2, 15, 16, 18] Figure 1b demonstrates the crystal structure of Cu_2O.

The third stable phase of copper-oxide with an atomic ratio of 1.33 is Cu_4O_3.[20] Cu_4O_3 is a mixed of Cu(I)/Cu(II) oxide. The local coordination environments of Cu(I) and Cu(II) are similar to the ones found in Cu_2O and CuO.[21] This less studied compound of the Cu_xO family was first discovered in 1870 as a mineral in the Copper Queen mine (Arizona, US).[2] Cu_4O_3 belongs to the tetragonal structure (space group, $I4_1/amd$) with a lattice constant of a = 5.837 Å and c = 9.932 Å.[21] Figure 1c demonstrates the crystal structure of Cu_4O_3. From the crystal structure, one can observe that there are two types of copper ion which are Cu^+ and Cu^{2+}. The Cu^+ has two oxygen atoms nearest neighbours forming collinear bonds of length 1.87 Å which is similar to cuprite (Cu_2O ~ 1.85 Å). Similarly, the Cu^{2+} is surrounded by four oxygen atoms with bond lengths and angles being very close to those observed in tenorite (CuO).[18, 19, 21] The crystallographic properties of Cu_4O_3 are tabulated in table 1.[2, 21, 22]

2.2 Electronic Band Structure

The reported band gap (E_g) values for CuO, which is a *p*-type semiconductor, are generally in the range of 1.2 to 2.16 eV.[1, 23-27] This wide range is attributed to several factors, including interpretation of the nature of the gap (i.e. direct or indirect), annealing treatment, grains dimensions, morphology and doping.[1, 25, 28-30] According to the Tauc relationship, for photon energies (E) greater than the band gap energy, the light absorption can be approximated using:[31]

$$\alpha E = \alpha_o \left(E - E_g\right)^{\eta} \quad (1)$$

where α is the absorption coefficient, α_o is a constant, E_g is the band gap energy and η is an exponent that depends on the type of transition involved. The value of η is $\frac{1}{2}$ or 2 for direct or indirect transitions, respectively. Rakhshani *et al*. have reported detailed studies of band gap determination of RF sputtered CuO films.[23] They found that their CuO films exhibited an indirect transition with a band gap of 1.21 eV. In contrast, Pierson *et al.* while reporting the same deposition technique (RF sputtering), determined their CuO films exhibited a direct band gap with a value of 1.71 eV.[32] The different values of E_g were due to different models ($(\alpha E)^2$ or $(\alpha E)^{\frac{1}{2}}$) being used to determine the band gap value. The other significant factor that contributes to the variation of band gap values of CuO films is related to the heat treatment. [29, 30] Izaki *et al.* demonstrated that annealing electrodeposited CuO films altered the E_g value.[29] They reported a reduction of 7.5% in E_g after annealing the as-deposited CuO at 773 K. They suggested that the changes in the composition, grain size and lattice constant were induced by the annealing process, altering the CuO band gap.[29]

In nanostructured CuO, the band gap generally increases with reducing crystallite dimensions.[1, 33] Experimentally, this is often observed as a blue shift of the optical absorption band-edge when the nanostructure dimensions are reduced. The blue shift can be attributed to the quantum confinement (QC) effect.[1, 34, 35] The strong QC effect occurs when the size of the crystal is reduced to much smaller than Bohr radius for the material (≈6.6 nm for CuO).[1] This causes direct changes to the electron wavefunctions and hence significantly alters the E_g. The weak QC effect occurs when the crystal size is larger than the Bohr radius. This causes indirect perturbation of the electron wavefunction due to Coulomb effects and results in more subtle changes in the band gap energy. [34, 35] In a recent study conducted by Rehman *et al.*, different scales of CuO nanoparticles, where the crystallite dimension is controlled by the annealing.[33] The crystallite dimensions obtained ranged from 11 nm (T = 250 °C) to 20 nm (T = 600 °C). They reported a reduction of 7% in direct E_g with an increase of crystallite dimensions.[33] In addition, it has been reported that the band gap values of the nanostructured CuO can be tuned *via* engineering the morphology[36-38] as well as doping[39-42].

Cu_2O is also a *p*-type semiconductor material due to the presence of copper vacancies.[2, 43] It is a direct band gap material with E_g > 2.1 eV. However the band gap can be tuned *via* engineering the grains dimensions. [24, 28, 30, 44, 45] This observation is widely attributed to the quantum confinement effect in smaller grains, causing a blue shift in the band gap.[34, 35, 46] In a recent study conducted by Poulopoulos *et al.,*[46] on Cu_2O thin films with thicknesses ranging from 0.75 to 5.4 nm the E_g value increased significantly from ~ 2.6 eV (5.4 nm film thickness) to ~ 3.8 eV (0.75 nm film thickness) due to quantum confinement effects. In addition, Balamurugan *et al* [45] and Chang Y *et al.*[44] also reported on the observation of quantum confinement effects in Cu_2O. They further studied the effect of temperature[45] and annealing duration[44] on manipulating the crystallite sizes and hence altering the band gap of Cu_2O.

Similar to CuO, the optical band gap of Cu_4O_3 has also been reported with a wide range of values from 1.34 to 2.47 eV which can also be attributed to the interpretation of the type of band gap and whether direct or indirect transitions are allowed.[20, 32, 47, 48]

A good comparison between the electronic properties of the three types of Cu_xO is presented via the band structure density functional theory (DFT) calculations by Heinemann *et al.* (Figure 2i).[19] Figure 2ii illustrates the Brillouin zones with special high symmetry k points of the three copper oxide compounds, which were used for the band structures DFT calculations.[19]

2.3 Optical Properties

The optical behaviours of Cu_xO films have been experimentally studied, in particular the complex dielectric function ($\varepsilon(E) = \varepsilon_1(E) + i\varepsilon_2(E)$) was determined *via* spectroscopic ellipsometry.[2, 49, 50] For comparison, the imaginary part (ε_2) of the dielectric function for CuO, Cu_2O and Cu_4O_3 are shown in Figure 3a,b with Gaussians fitting marked with numbers 1 to 7. For Cu_2O the peaks originate from the various band gaps corresponding to 2.59 eV (1), 2.71 eV (2),…and 5.24 eV (7).[2] The difference in energy between these two first peaks is attributed to the spin–orbit–splitting energy of ~0.12 eV for Cu_2O.[49] The absence of any sharp peaks for the CuO (ε_2) spectrum is due to low symmetry of this crystal. Similarly no sharp peak is seen for Cu_4O_3 for energies of less than 3.7 eV.

There are many reports regarding the absorption coefficient $\alpha(E)$ and normal–incidence reflectivity $R(E)$ of Cu_xO films in optical ranges.[2, 49-51] Cu_2O is expected to have an essentially full Cu 3d shell with a direct forbidden band gap of 2.17 eV in bulk, which can only absorb light up to the visible region. In contrast, CuO has an open 3d shell with a direct band gap (1.2 eV in bulk) of charge-transfer type, which can absorb light up to the near infrared (IR) region.[1, 15, 27] A detailed analysis of the absorption coefficient obtained on bulk and thin film Cu_2O can be found in the report by Marleba *et al.*[51] Additionally, Rehman *et al.* and Borgohain *et al.* reported the optical absorption properties of CuO and Cu_2O nanoparticles of different sizes, respectively.[33, 52] A comparative study of optical absorption between nanoparticles and near-monodisperse nanospheres of Cu_2O has been reported by Zhang *et al.*[53] They found that the nanospheres of Cu_2O have a wide absorption peak at 520 nm while Cu_2O nanoparticles have an absorption edge at 550 nm.[53]

Mayer *et al.* have reported that CuO is nonluminescent.[2] This is despite a few reports demonstrating the photoluminescence (PL) of CuO films, however the purity of such films is questionable (the presence of Cu_2O is a possibility). Nevertheless, Zhang *et al.* reported a detailed analysis of the PL properties of CuO nanostructures. They found that the PL properties of nanostructured CuO can be controlled *via* altering their shape, dimension and morphology.[1] The QC effect and specific surface effect are the two most reported mechanism which can result in the blue shift and red shift of the PL peak, respectively.[1, 54] On the other hand, Cu_2O shows a weak PL effect due to the fact that optical transitions require parity change, which does not exist between the energetically highest valence band and lowest conduction band of the Cu_2O direct transition band.[2] In bulk Cu_2O, there are three peaks or shoulders that can be assigned to doubly charged oxygen vacancies (V_O^{2+}) at 1.72 eV (720 nm), singly charged oxygen vacancies (V_O^{1+}) at 1.53 eV (810 nm) and copper vacancies (V_{Cu}) at 1.35 eV (920 nm).[2] In nanostructured Cu_2O, these peaks and shoulders can be tuned *via* shape, dimension and morphology alterations as observed by Shi *et al.*[55, 56]

2.4 Vibrational Properties

The lattice dynamics of Cu_xO materials have been studied using IR, Raman and photoluminescence spectroscopy.[57-61] These studies provided insight into the nature of the electron phonon interaction and the negative thermal expansion (NTE) in Cu_xO. These methods also provided information about spin–phonon interaction and size dependent electron phonon scattering.[61] Debbichi *et al.* reported an extensive study of vibrational properties of Cu_xO *via* Raman spectroscopy where they clearly distinguished the different types of vibrational modes either by Raman and IR spectroscopy.[61] Recently, Shih *et al.* have reported studies on the size effects of spin-phonon coupling in in-plane CuO nanowires.[62] They employed low-temperature Raman spectroscopy for probing the local atomic vibrations of nanowires. They found that the spin-phonon mode varies with the size of the CuO nanowires due to the increase in the strength of spin-phonon coupling.[62]

The IR spectroscopy modes are associated with the relative motion of both copper and oxygen atoms which consist of asymmetric Cu–O stretching and asymmetric O–Cu–O bending modes. In contrast, Raman active modes only involve the relative motion of oxygen atoms.[63] Figure 4 shows Raman spectra of Cu_xO with calculated frequencies of Raman active vibrational modes.[61] The symmetries of the zone–center modes are given by the following representations:[2, 61]

$$\Gamma_{Cu_2O} = A_{2u} + E_u + 3T_{1u} + T_{2u} + T_{2g} \quad (2)$$

$$\Gamma_{CuO} = A_g + 2B_g + 4A_u + 5B_u \quad (3)$$

$$\Gamma_{Cu_4O_3} = 3E_g + A_{1g} + 2B_{1g} + 9E_u + 6A_{2u} + 5B_{2u} + 2B_{1u} + 2A_{1u} \quad (4)$$

2.5 Electrical Properties

The electrical conductivity and hole density of *p*–type Cu_2O films vary with copper vacancy density, which act as shallow acceptors.[2] Similarly in CuO, copper deficiencies account for the intrinsic *p*–type semiconducting behaviour.[64] Suda *et al.* and Young *et al.* have studied the effect of temperature on electrical conductivity of CuO and Cu_2O films, respectively (Figure 5 a,b).[65, 66] They have shown that an increase in temperature increases the conductivity of CuO and Cu_2O due to an increase in hole concentration.[65] Similar findings were also reported by Gopalakrishna *et al.*[67] using Hall effect studies. They revealed a significant increase in conductivity, mobility and carrier concentration of nanocrystalline CuO after annealing.[67] Apart from temperature, electrical properties of Cu_xO are also relied on grain dimensions, grain boundary, film thickness, specific phase and dopants.[1-3, 68-72] Shao *et al.* reported an electrical conductivity of individual single CuO nanowires grown by thermal oxidation.[69] The electrical transport measurement has shown that the CuO nanowire has a conductivity of 7.8×10^{-4} $(\Omega\ cm)^{-1}$.[69] Additionally, Liao *et al.* reported an individual Cu_2O nanowires has a high mobility of $> 95\ cm^2\ V^{-1}s^{-1}$.[70] It is possible to tune the electrical properties (resistivity, carrier concentration and mobility) of Cu_xO by changing the stoichiometry and crystallinity of the Cu_xO films during the deposition process. Deposition parameters, such as pH of the solution in electrodeposition and hydrothermal methods and ion pressure and concentration in RF sputtering techniques, significantly contribute to changes in stoichiometry and crystallinity.[73-75].

2.6 Thermal Properties

A limited number of studies have been carried out on the thermal properties of pristine copper oxides films. However, great interest has been shown for the development of nanoparticles of Cu_xO suspensions in fluids (nanofluids) due to the significant enhancement of thermal conductivity that they grant to the fluid in which they are suspended.[76-79] The relatively high thermal conductivity of the CuO (76.5 W/mK)[78], makes it an excellent candidate for enhancing the efficiency and reliability of refrigeration and air conditioning systems.[80, 81] In contrast, Cu_2O has a rather low thermal conductivity of the order of 4.5 W/mK.[82, 83] It has been shown that the thermal conductivity enhancement of both CuO and Cu_2O nanofluids correspond to an increased particle volume fraction and temperature.[84-87]

The variations in the Seebeck coefficient (S) of CuO and Cu_2O as a function of temperature are shown in Figure 5a,c for which both oxides show decreasing trends. It has been shown that at 500 K, CuO and Cu_2O exhibit a maximum value of 200 μV/K and 1050 μV/K, respectively.[65, 66]

The presence of a wide gap in the phonon spectra between low frequency (due to acoustic and optical phonon modes that involve the motion of Cu atoms) and high frequency (due to the optical modes of oxygen vibrations) bands are reflected in the temperature dependence of heat capacity.[88] The calculated and experimental heat capacities (C_p) of CuO and Cu_2O as a function of temperature are shown in Figure 5d,e.[88-93] As seen from the Figure, the shape of C_p *vs* temperature curves for both CuO (for temperatures below 800 K) and Cu_2O (for temperatures below 500 K) are accurately accounted for by the calculations that employ the quasi–harmonic approximation.[88]

2.7 Magnetic Properties and Superconductivity

The copper–oxygen covalent bond is the prominent factor governing the properties of high transition temperature (High-T_c) superconducting Cu_xO compounds.[94] Both CuO and Cu_4O_3 have an antiferromagnetic ground state. For CuO the antiferromagnetic unit cell has twice the size of the primitive unit cell of the crystal.[19] In the case of Cu_4O_3, it was suggested that the antiferromagnetic unit cell doubles the crystallographic unit cell in all three special directions.[19, 95-97] Bulk CuO is antiferromagnetic with Néel temperatures from 213 K to 230 K.[1, 98, 99] The CuO antiferromagnetic transition takes place in two stages: near 230 K it leads to incommensurate antiferromagnetic order and near 213 K by a first order transition to a commensurate antiferromagnetic order.[94] As mentioned in section 2.1, the copper atom of CuO is surrounded by four coplanar oxygen atoms, resulting in two sets of one dimensional Cu–O chains. The magnetic interaction due to super exchange leads to antiferromagnetic order in the Cu–O–Cu chains along the $[10\bar{1}]$ direction with a bond angle of 146°.[94] Magnetic properties of nanostructured CuO significantly rely on their grain dimensions, morphology as well as anisotropy of the nanostructures.[1] A diameter of 10 nm is a critical size for CuO nanoparticles to show a ferromagnetic behaviour.[1, 100-102] Interestingly, there are reports regarding room-temperature ferromagnetism of pure CuO nanostructures.[1, 103-105] The room-temperature ferromagnetism is due to oxygen vacancies at the surface/or interface of the nanoparticles.[1, 105]

A neutron diffraction study revealed that Cu_4O_3 undergoes a magnetic phase transition below 42.3 K leading to a pyrochlore lattice.[95, 96] The amplitude of the magnetic moment carried by Cu^{2+} is ~0.46 μ_β which indicates the strong covalent character of the Cu–O bonds and the presence of strong fluctuations even at low temperatures.[95]

Compounds made of Cu and O are the base of a famous class of high–T_c superconductors.[94] Superconductivity in these materials is observed when they are strongly doped away from their ideal stoichiometry. It has been shown that spatial changes in carrier density and superconducting gap produce local inhomogeneity, which strongly affects their superconductivity.[106]

High–T_c was first discovered by Bednorz and Müller in 1986 using Cu and O compounds such as La_2CuO_4 doped with Ba.[107] A few months later it was found that doping the same material with Sr raised the superconducting critical temperature to nearly 40 K.[107] Recently, the performance of high-T_c copper and oxygen based materials were further enhanced with the inclusion of extra oxygen atoms as mobile "holes" into the copper oxide planes as illustrated in the $Bi_2Sr_2CaCu_2O_{8+x}$ and $YBa_2Cu_3O_{6+x}$ systems.[106, 108] Apart from providing charge carriers, the role of oxygen dopants is still debatable and being investigated.[106, 108-110]

2.8 Doping

It is possible to modify the chemical and physical properties of Cu_xO through doping. It has been shown that doping has the capability to alter the conduction type of Cu_2O (from p to n). Based on the valence of Cu and O, which are +1 and –2 in Cu_2O, some n–type dopants including group VII elements such as halogens (O sites) (and possibly group II elements (Cu sites)) allow this transition to occur.[111] The typical reported halogen dopants include flourine (F), chlorine (Cl) and bromine (Br) which can be intercalated into the structure of Cu_2O during the synthesis process.[111-114] Theoretically, F is the best match for O given the similarity in size; however, CuF is soluble in water.[111] Recently, Scanlon *et al.* have demonstrated that intrinsic n-type defects or defects complexes in Cu_2O created during an electrodeposition process cannot be the source of any n-type behaviour.[75] They have suggested that the n-type conduction is due to an inversion layer which was attributed to a shallow donor level being formed during the electrodeposition process or due to external impurities (dopants).[75]

Generally, the hole density of native p–type Cu_xO films are poor, uncontrollable and sensitive to the preparation methods and experimental conditions. It has been reported that nitrogen (N) and silicon (Si) doped Cu_2O *via* a RF sputtering process can significantly reduce such instabilities.[115-118] These dopants were found to act as acceptors, which are incorporated into the oxygen lattice without converting the conduction type of Cu_2O.[117, 118] To further stabilize the films Ishizuka *et al.* and Okamoto *et al.* investigated the effect of passivation using hydrogen (H) and crown–ether cyanide of the N doped Cu_2O films.[115, 119] The improvement after the treatment indicates that hole traps are passivated by the cyanide or protons. These holes traps are generally due to oxygen vacancies or dangling bonds of Cu.[115]

For solar cells applications, the intrinsic photoconductivity of Cu_2O can be limited by minority charge carrier recombination caused by native defects acting as trap states. Isseroff *et al*. used first principles DFT calculations to study these trap states and demonstrated that substitutional cation doping reduces the recombination effect.[43] They found that split vacancies are the source of trap states that inhibit the minority carrier diffusion in Cu_2O. Dopants such as lithium (Li), magnesium (Mg), manganese (Mn), and zinc (Zn) prevent the formation of the split vacancies for a single cation vacancy which resulted in an electronic structure that exhibited no trap states within the band gap.[43]

3.0 NANOSTRUCTURED Cu_xO SYNTHESIS

Many different approaches for the synthesis of nanostructured Cu_xO have been implemented using both vapour and liquid-phase-based methods. In this section, we present the most common synthesis methods and describe how they can be employed for engineering and tuning the morphologies and properties of Cu_xO.

3.1 Vapour phase Synthesis

Vapour phase synthesis methods can be divided into two different categories: (i) physical vapour deposition (PVD) and (ii) chemical vapour deposition (CVD). The main difference between them is the process they employ, in which PVD uses physical forces to deposit films, while CVD uses chemical processes.

3.1.1 PVD methods

Many of the common PVD synthesis techniques such as RF sputtering, direct current (DC) sputtering, thermal evaporation, thermal oxidation, molecular beam epitaxy (MBE), pulse vapour deposition (PLD) and electron beam epitaxy (EBE) have been used for the deposition of nanostructured Cu_xO. A PVD process is purely physical, starting with either Cu_xO or Cu as the source material in the form of a solid target or powder, which is evaporated or sputtered with the application of ion bombardment, thermal heating, electron beam impingement or laser irradiation.

3.1.1.1 Sputtering

Amongst the PVD techniques, sputtering has, thus far been the most common technique to synthesize thin films Cu_xO, due to the ease of control over the deposition parameters. The as-synthesized films usually exhibit nanometer-sized tightly packed columnar structure.[120-125]. Sputtering is a process in which atoms are ejected from a solid target material by bombarding it with energetic particles. It offers a high degree of control over a film's crystallinity and stoichiometry. The crystallinity, grains dimension and stoichiometry of the copper oxides films can be controlled by varying the sputtering parameters such as applied power, oxygen flow rate, oxygen partial pressure and concentration as well as annealing temperature.[32, 120-122, 124-128] For example, Chu *et al.* reported crystallite sizes of Cu_2O thin films changed from 16.8 to 8.8 nm when oxygen partial pressures increased from 1.1×10^{-3} to 1.8×10^{-3} Torr. This indicated that the higher the oxygen partial pressure, the smaller the crystallite size in the nano-crystalline Cu_2O thin films.[120] In contrast, Elfadill *et al.* reported the crystallite size of CuO increased from 12 to 24 nm as the oxygen pressure increased.[125]

Generally in an oxygen rich sputtering chamber, at relatively low sputtering powers, only a small number of Cu atoms are sputtered, which effectively react with oxygen in the plasma, resulting in the deposition of films with high oxygen content such as CuO films. Conversely, Cu_2O films are formed at high sputtering powers, due to a large number of sputtered Cu atoms.[122, 126] However, relatively high sputtering powers can also adversely affect the stoichiometry of the films, resulting in presence of unreacted metallic copper and undesirable stoichiometric ratios between copper and oxygen.[122]

Although Cu_4O_3 was discovered during the late 1870s, the synthesis of single phase Cu_4O_3 thin films has rarely been reported. Pierson *et al.* and Richthofen *et al.* have successfully demonstrated the synthesis of single CuO, Cu_2O and Cu_4O_3 phases by varying the oxygen flow rate using a reactive magnetron sputtering technique.[32, 128] They used a Cu target with the RF power maintained at 600 W. It was suggested that conductive Cu−rich copper oxide (Cu_4O_3) thin films tended to form with an oxygen flow rate $R(O_2) < 30\%$, whereas insulator O−rich copper oxide (CuO) thin films tended to form at $R(O_2) \geq 30\%$.[129] This is in contrast to the work of Blobaum *et al.* whom also successfully synthesized Cu_4O_3 films *via* the sputtering, but with a CuO target and at a lower sputtering power of 200 W.[127]

3.1.1.2 Thermal Evaporation

Deposition of Cu_xO films using thermal evaporation is achieved by vaporizing a source material of Cu or Cu_xO (in either powder or condensed form) using heat either in a vacuum or in a controlled gaseous environment at a low pressure.[25, 45, 130-133] The vaporized Cu or Cu_xO that emanates from the material source interacts with the gas molecules in the environment of the deposition chamber before condensing onto a substrate. Processing parameters such as evaporation temperature, substrate temperature, substrate type, gas environment and pressure all play important roles in achieving the desirable Cu_xO thin films.[25, 131, 134] It has been reported that the as-synthesized Cu_xO films from these methods are usually compact thin films, which are textured by nanocrystallites (25 – 30 nm).[25, 45, 132, 133]

3.1.1.3 Thermal Oxidation

Thermal oxidation techniques offer a simple, convenient and fast method to synthesize nanostructured Cu_xO with various morphologies including nanowires, nanoribbons and nanorods.[135-139] In this method nanostructured Cu_xO is directly grown on the surface of a Cu substrate.[137, 138, 140] Thermal oxidation is performed by simply heating a Cu substrate to a high temperature (typically between 200 and 800 °C) in an oxygen rich environment.[135, 137, 138, 141-143] Generally, the morphology and stoichiometry of the Cu_xO can be controlled by tuning the deposition parameters. For instance, the diameter and density of Cu_xO nanowires can be altered by changing the oxidation temperature.[144] However, very high oxidation temperatures (> 900º C) are not suitable for nanowire formation as Cu_xO nanostructures can be fused together, as

observed by Huang *et al.*[145] Valladares *et al.* have studied the effect of oxidation temperature in altering the stoichiometry of the Cu_xO films. They have observed that pure Cu_2O films are obtained at 200 °C, whereas CuO films are obtained above 300 °C.[143]

Unfortunately, mechanical adhesion between the as-deposited nanostructured Cu_xO and the substrates synthesized by the thermal oxidation method is very weak.[143, 146-149] Cracking and flaking of the Cu_xO films or even exfoliation from the substrates posed a big challenge which severely affects the properties and practical applications of the nanostructured Cu_xO. Several methods have been proposed to alleviate the cracking and flaking problem including pre-deposition of a ZnO layer on copper foil[150], synthesis of CuO nanowires on other foreign substrates such as silicon[147, 151] or glass[152] and synthesis of CuO nanowires on porous substrates such as porous copper substrate[149] or nickel foam[148] as shown in Figure 6. Zhang *et al.* have successfully demonstrated non cracked and flaked CuO nanowires synthesized on porous copper substrates. The porous substrates managed to reduce thermal stress during the oxidation process and as a result eliminate cracking and flaking issues.[149]

3.1.1.4 Other PVD methods

Apart from the aforementioned vapour phase methods, PLD[153-157] and EBE[158-161] deposition techniques are the other alternatives available for synthesizing Cu_xO films. It has been reported that the as-synthesized Cu_xO from these methods are usually compact thin films, which are textured by nanocrystallites (10−800 nm). The dimensions of the crystallites are significantly affected by the oxygen pressure and substrate temperature which were identified as being the two most important parameters.[154, 155]

3.2 CVD methods

CVD processes have become popular deposition techniques owing to their inherent flexibility and potential to tailor the Cu_xO phase composition by simply varying the operating conditions and precursors. Many forms of CVD have been used for depositing different Cu_xO stoichiometries, including atmospheric pressure CVD,[13, 162, 163] aerosol assisted CVD,[164-167] and plasma assisted CVD.[168] Such films are typically of compact structure, consisting of micro- or nanometer-sized grains.

Generally, precursors such as bis–(2,4–pentanedionato) copper (II) or $Cu(acac)_2$ (acac = acetylacetonate) are used due to their high sublimation rate (activation energy of 105.6 kJ mol^{-1}) and low sublimation temperature between 140 to 190 ºC.[162] Valtierra *et al.* have demonstrated the synthesis of nanostructured Cu_4O_3 and CuO thin films with crystallite size of 6.5 to 8.4 nm on fiberglass substrates using $Cu(acac)_2$ as a precursor and oxygen as a carrier-reactant gas *via* atmospheric pressure CVD.[162] The deposition temperature of CuO and Cu_4O_3 were recorded at 315 ºC and 345 ºC, respectively. In addition, thin films of Cu_2O have also been synthesized on fiberglass substrates using a similar technique and precursors by Ortiz *et al.* at a deposition temperature of 320 ºC.[163]

However, precursors such as $Cu(acac)_2$, $Cu(dpm)_2$ (dpm = dipivaloylmethanate) and $Cu(hfa)_2$ (hfa = hexafluoroacetylacetonate) may present drawbacks in terms of poor thermal characteristics, reduced shelf life, halide incorporation or instability upon prolonged utilization due to aging phenomena.[169] Therefore, a second generation of adducts of the type $M(hfa)_2$• tetramethylethylenediamine(TMEDA) (M = Cu(I) or Cu(II)) have been successfully adopted as alternative precursors.[169] They have favourable properties in terms of improved long–term stability and volatility with respect to conventional β–diketonate.[13, 169] Barreca *et al.* were the first group to successfully demonstrate the deposition of nanostructured CuO and Cu_2O using $Cu(hfa)_2$ adduct with TMEDA *via* CVD.[169] They successfully demonstrated morphological evolution from continuous films to 1D hyperbranched nanostructures.[169]

Spray pyrolysis is a typical aerosol-assisted chemical vapour deposition, which is utilized in the glass industry and in solar cell production to deliver film coatings of various thicknesses.[34] This method has the benefit of forming large-scale thin films by using a simple apparatus that can lead to increase productivity. Moreover, the film thickness and stoichiometry are easy to control and the resulting films are generally dense.[165, 166] During film deposition, the precursor's solution is pumped to an atomizer, and then sprayed onto heated substrates. Subsequently the droplets undergo evaporation, solute condensation and thermal decomposition, which results in film formation.[34] The composition of these thin films is highly dependent on the solvent, morphology of the substrate as well as the deposition temperatures.[164, 170]

Cu_xO films generated by the spray pyrolysis method are generally produced from copper acetate or copper nitrate as precursors dissolved in alcohol based solutions such as ethanol, propanol or methanol.[164, 166, 170, 171] Alcohols are used to increase the wettability of the sprayed solution on the substrate and to improve the homogeneity of the deposited films.[165] It has been reported that Cu_xO nanostructures form with the addition of glucose or sucrose to the solution.[165, 167] These sugars are used as reducing agents in the precipitation of the Cu_xO nanostructures.[165] Waser *et al.* demonstrated synthesis of CuO nanoparticles *via* flame spray pyrolysis with various diameter from 6 to 50 nm by varying precursor solution and oxygen flow rate.[172]

Apart from CuO and Cu_2O films, Cu_4O_3 films can also be obtained *via* spray pyrolysis techniques. Albores *et al.* have successfully demonstrated the deposition of Cu_4O_3 films on ZnO nanorods.[170] The formation of Cu_4O_3 films is a gradual process. Initially, the possible lattice matching of ZnO and CuO promotes the growth of CuO. In the presence of methanol, at elevated temperatures, the Cu^{2+} in CuO is reduced to Cu^{1+} forming Cu_2O as:[170]

$$CH_3OH_{(g)} + 6CuO \rightarrow 3Cu_2O + CO_{2(g)} + 2H_2O_{(g)} \quad (5)$$

Then at these elevated temperatures, the solid reaction between CuO and Cu_2O results in paramelaconite phase formation which can be described by:[170]

$$2CuO + Cu_2O \rightarrow Cu_4O_3 \quad (6)$$

3.3 Liquid phase synthesis

Liquid phase techniques include methods such as electrodeposition, hydrothermal/solvothermal and sol–gel. These methods are generally chosen due to their low capital cost and better control of the material's morphology in comparison to vapour phase deposition techniques as well as

the deposition at relatively low temperatures, which is crucial for low-heat-tolerant substrates. Among a variety of liquid phase synthesis methods, hydrothermal/solvothermal and chemical precipitation techniques have been widely used to synthesize Cu_xO nanostructures.

3.3.1 Electrodeposition

Electrodeposition is a process in which metal ions in an electrolyte are reduced at a conducting electrode under potential control. The process uses electrical current to reduce Cu^{2+} ions from an aqueous solution. The electrolyte generally contains a mixture of a Cu salt such as copper sulphate, copper acetate or copper nitrate and a chelating agent such as lactic acid, ammonium nitrate, amino acids or tartaric acids.[29, 173-177] The deposition is carried out in alkaline environment with the addition of sodium hydroxide or ammonia to control the pH level. The electrodeposition technique is commonly used for depositing CuO and Cu_2O films.[3, 29, 173-175, 177-180] Such films are typically of compact structure, consisting of micro- or nanometer-sized grains. The stoichiometry of the electrodeposited films is very much dependent on the type of the chelating agent and applied potential used during the electrodeposition process. Generally, CuO films are obtained upon the application of a positive voltage/current bias, where oxidation of Cu is expected and this process is well known as anodic electrodeposition. Inversely, Cu_2O films are deposited at a negative bias, in which the reduction process occurs (cathodic electrodeposition).[173, 174, 181]

Synthesis of CuO films *via* anodic electrodeposition in an alkaline solution containing copper (II) nitrate, ammonium nitrate and ammonia has been reported by Izaki *et al.* at +0.9 V *vs* Ag/AgCl.[174] Sasano *et al.* demonstrated that CuO films formed by applying potential pulses are more crystalline than the ones deposited using a constant potential.[176] The mechanism for the electrodeposition of CuO films is outlined in equations (7)–(10). The reaction starts *via* electrolysis of water to generate oxygen and protons (reaction 7). Consequently, these protons react with ammonia Cu(II) complexes to yield free Cu(II) ions in the vicinity of a substrate's surface (reaction 8). The free Cu(II) ions are then hydrolyzed to form CuO films on the substrate (reactions 9 and 10).[174, 181]

$$2H_2O \rightarrow O_2 + 4H^+ 4e^- \quad (7)$$

$$Cu(NH_3)_4^{2+} + 4H^+ \rightarrow Cu^{2+} + 4NH_4^+ \quad (8)$$

$$Cu^{2+} + 2OH^- \rightarrow Cu(OH)_2 \quad (9)$$

$$Cu(OH)_2 \rightarrow CuO + H_2O \quad (10)$$

Similarly, syntheses of Cu_2O films have been reported *via* cathodic electrodeposition using an alkaline aqueous solution containing copper (II) sulphate or copper (II) acetate and lactic acid as the chelating agent.[10, 173, 175, 179, 180, 182] Zoolfakar *et al.* have demonstrated the electrodeposition of Cu_2O films onto ZnO for forming heterojunction solar cells.[173] The electrodeposition process was carried out at –0.55 V *vs* Ag/AgCl. Cu_2O was formed according to the following electrochemical reaction.[175]

$$2Cu^{2+} + 2e^- + 2OH^- \rightarrow Cu_2O + H_2O \quad (11)$$

Apart from depositing thin films Cu_xO, electrodeposition techniques have been used to synthesize various morphologies of nanostructured CuO and Cu_2O including leaf-like[183], nanospindles[184], nanocubes[185], nanorod[186] and cauliflower-like[187]. Interestingly, Seigfried and Choi have demonstrated a new level of tuning and engineering the morphology of Cu_2O crystals *via* electrodeposition technique.[188, 189] They manipulated deposition parameters such as potential and current to engineer to Cu_2O crystals as illustrated in Figure 7.[189]

3.3.2 Hydrothermal and Solvothermal

Hydrothermal and solvothermal processes are facile and cost-effective deposition techniques. They have the capability of producing nanostructured Cu_xO of different morphologies including nanodendrites,[190] nanowires,[71] nanorings,[191] nanorods,[192-195] nanoribbons,[191, 194] nanotubes,[192] microspheres[194, 196] and macrowhiskers.[197] (Figure 8)

The synthesis of nanostructured Cu_xO has been hydrothermally achieved using various precursors such as copper (II) chloride, copper (II) acetate or copper (II) sulphate. Generally, a lower concentration of $Cu(OH)_4^{2-}$ precursors favours tubular formation, whereas a higher concentration leads to rodlike morphologies.[192, 194] In most cases, the hydrothermal synthesis of Cu_xO starts with the preparation of a solution that contains copper salts, sodium hydroxide and solvents, typically deionized water. Such a solution is then kept at an elevated temperature (100 – 300 ºC) for a certain period of time, allowing the nucleation and growth of Cu_xO crystallites.

Solvothermal methods are almost identical to hydrothermal methods except that organic solvents are used instead of water.[198, 199] In comparison with the hydrothermal method, the solvothermal method exhibits many advantages such as easier morphological control, free foreign anions and macroscopic quantity.[200, 201] Recent reports have shown that high-aspect-ratio of Cu_xO nanostructures can be synthesized *via* solvothermal methods.[202-205] Zhao *et al.* have demonstrated a facile method to synthesize pure polycrystalline Cu_4O_3 microspheres using copper (II) nitrate as the precursor in the presence of *N,N*−dimethylformamide and ethanol.[201] They have successfully manipulated the CuO/Cu_2O stoichiometry ratio to generate Cu_4O_3 films with the reaction of $(2CuO + Cu_2O \rightarrow Cu_4O_3)$ in a closed system.[201]

3.3.3 Solution-based Chemical Precipitation Methods

In most cases, the chemical precipitation synthesize of CuO nanoparticles starts with the preparation of a solution that contains copper salts, sodium hydroxide and solvents, typically deionized water. In order to avoid agglomerate of the CuO nanoparticles, an external energy such as ultrasonic or high pressure need to be applied during the synthesize process. Zhu *et al.* prepared highly dispersed CuO nanoparticles of 6 nm with various morphologies including spherical, ellipsoidal and needle-shape CuO.[206] Wu *et al.* prepared CuO nanoparticles with different sizes and morphologies in organic solvents such as dimethylacetamide (DMAC).[207] They found that the nucleation and growth kinetic of CuO nanoparticles can be tuned by varying the processing parameters including the volume ratio of DMAC and water, increasing the temperature of the solution and the molar ratio of Cu^{2+} and OH^-.[207] Apart from nanoparticles, chemical precipitation synthesis has commonly used to synthesize different morphologies of CuO

including nanowires[208-210], nanoribbons[211], flower-like[212, 213], hierarchical nanochains[214] and nanosheets[215, 216]. Recent comprehensive review on nanostructured CuO *via* solution-based chemical precipitation technique is found elsewhere.[1]

There are many reports of synthesis of nanostructured Cu_2O *via* chemical precipitation.[53, 217-224] Gou *et al.* demonstrated a synthesis of highly uniform and monodisperse Cu_2O nanocubes. The process involved the use of sodium ascorbate to reduce Cu(II) salts in water, in the presence of a surfactant and NaOH. The nanocubes dimensions were tuned by varying the concentration of the surfactant.[217] Zhang *et al.* reported synthesis of monodisperse Cu_2O and CuO nanospheres. It has also been shown that by modulating the concentration of solvent, the diameter, crystallization and monodispersity of Cu_2O nanospheres can be kinetically controlled.[53] Interestingly, various groups have reported facile method for the synthesis of Cu_2O nanocrystals with systematic shape evolution (Figure 9).[220-223] Recently, Susman *et al.* demonstrated precise morphology control of Cu_2O nanocrystals covering the entire range of morphologies from complete cubes, *via* the intermediate morphologies truncated octahedral, cuboctahedra and truncated cubes, to complete octahedral.[220] The highly effective morphology control is attributed to competitive adsorption of hydroxide and citrate anions on the [100] and [111] planes of the growing crystallite.[220]

3.3.4 Other film formation methods

A sol–gel process involves the formation of a colloidal solution (sol) from selected chemicals that acts as a precursor for an integrated network (gel) of either discrete particles or connected networks. During the gelation (aging process), various forms of hydrolysis and polycondensation processes can take place. Film deposition is generally carried out during the gelation process *via* dip-coating, spin coating or drop–casting onto the substrates. Armelao *et al.* have reported Cu_xO thin films *via* sol–gel synthesis, using ethanolic solutions of copper (II) acetate.[225] Films were obtained by dip–coating at room temperature in air and were subsequently heat−treated at different temperature (100–900 ºC) in oxidizing (air), inert (N_2) or reducing (4% H_2 in N_2) atmospheres to observe different crystalline phases of Cu_xO as a function of the annealing conditions with an average crystallite size lower than 20 nm.[225] Ray has also reported a similar technique, however he experimented with methanolic solutions of cupric chloride.[226] Under an atmospheric heat-treatment condition, Armelao *et al.* have only managed to observe the CuO phase with 900 ºC annealing, while Ray has successfully demonstrated the deposition of CuO and Cu_2O at 360 ºC and 400-500 ºC, respectively.[225, 226]

Templating is a modification of the sol−gel synthesis technique and can be very effective for the preparation of Cu_xO nanowires.[141] Nanostructured Cu_xO is deposited onto porous templates such as anodic alumina membranes and polycarbonate membranes.[227-229] Generally, templates are used for assisting the growth of the Cu_xO by controlling the diameters, lengths and densities of the nanowires.[227] At the end of the deposition process, the templates must be removed either by chemical reactions[229] or a selective burn-away at high temperatures[230]. Consequently, this procedure may prolong the process as well as degrade the quality of the Cu_xO.[141]

4.0 APPLICATIONS Cu_xO

Cu_xO has been employed for a variety of applications ranging from optical devices to high thermal conductivity systems. In this section, some of the most common applications of Cu_xO materials are presented. Particular emphasis is placed on the enhancements that can be achieved by exploiting the nanostructured forms of Cu_xO.

4.1 Solar Cells and Light Emitting Diodes

Cu_xO films are possible candidates for developing different types of optical devices, including solar cells based on dye−sensitized and heterojunction architectures as well as organic light emitting diodes.

The quest and need for a clean and economical energy source have increased interest in the development of solar applications. Amongst various metal oxide materials for solar energy applications, Cu_2O has attracted increasing interest due to its theoretical power conversion efficiency (PCE) of 18% and an absorption coefficient higher than single crystalline Si.[173, 231]

As described previously Cu_xO is an intrinsically *p*-type material. However, self−compensation problems and dopant solubility have inhibited the synthesis of *n*−type Cu_xO to produce efficient homojunctions for photovoltaic applications.[3, 72, 232] Therefore, heterojunction architectures have been employed with other *n*−type semiconductors such as ZnO,[10, 173, 175] CdO,[233] TiO_2,[234-236] Ga_2O_3[237] and GaN.[2] Amongst the aforementioned *n*−type semiconductors, ZnO has been found to be the most stable and exhibit relatively low lattice mismatch of 7.6% between the (002) ZnO and (111) Cu_2O phase.[3, 175, 177] Despite the predicted PCE value of 18%, in practice the ZnO−Cu_2O solar systems have yet to reach high efficiencies.[3, 10, 238] To date, the highest efficiency ever reported for bilayer ZnO−Cu_2O heterojunction solar cells has been 3.83%.[239] This is due to the fact that theoretically their intrinsic electronic band structures do not permit an open circuit voltages larger than 0.7 V.[238] To date, the largest ever short circuit current that has been reported by Zoolfakar *et al.* using electrodeposited ZnO and Cu_2O films was 12.7 mA cm^{-2} (Figure 10).[173]

Apart from heterojunction cells, Cu_xO has also been widely used in dye−sensitized solar cell (DSSC) technology. CuO is commonly used as a blocking layer that prevents recombination reactions by forming a potential barrier between the anode and the electrolyte which enhances the PCE of the device.[240-243] Yet in other experiments, the use of Cu_2O at the photoanode of a DSSC was found to decrease the overall PCE.[244] This is due to dissociation of copper in liquid−based electrolytes, inducing numerous extrinsic defects that increases carrier recombination, resulting in photovoltaic performance degradation.[244]

Cu_xO has also been used in organic light emitting diodes (OLEDs).[134, 245] In order to construct efficient OLEDs, it is important to optimize the carrier injection ability at the interface of the active layer and anode materials. The Cu_xO films are commonly used as hole injection layers (HILs) to lower the hole injection barrier.[134, 246, 247] Kim *et al.* have reported the advantage of using a mixed stoichiometry of CuO and Cu_2O for increasing the performance of OLEDs as illustrated in Figure 11.[134] Mixed stoichiometry of Cu_xO contains high density of defects such as oxygen vacancies or unbonded oxygen atoms, which act as an extra energy state within the energy gap of the Cu_xO layer. Interestingly, when

the energy levels of these gap states are aligned with the highest occupied molecular orbital (HOMO) level of the hole transporting layer, no potential barrier is produced at the anode interfaces, which can lead to an increase in the hole injection efficiency.[134]

4.2 Photo–catalytic Applications

Cu_xO is a promising photo–catalyst that is used in many chemical processes, such as organic contamination degradation and water splitting under visible–light irradiation owing to their small band gap and low cost.[13, 248-255] Under illumination, Cu_xO produces electron/hole pairs that can generate hydroxyl radicals ($^{\bullet}HO$) from water. This radical is capable of mineralizing most organic molecules.[250] For water splitting applications, the majority charge carriers of the Cu_xO (holes) oxidize water to oxygen gas (O_2), while the photo–generated minority charge carriers (electrons) reduce water to hydrogen gas (H_2).[248, 254, 255] Significantly, the Cu_xO conduction band is more negative than the redox potential of H^+/H_2, which allows sunlight to produce H_2 from water. [253]

Unfortunately, the general photo–instability of Cu_xO greatly hinders its direct application in photo–catalysis.[248, 256] To overcome this photo–instability effect, Cu_xO is typically coupled with other semiconductors to form heterojunctions and it has been reported that TiO_2 is one of the best candidates for this purpose.[256, 257] Additionally, nanostructuring of Cu_xO can also significantly improve overall stability.[256] Fortunately, the large surface area to volume ratio, which is provided by nanostructuring, significantly increases the effective surface area available for photo–catalytic reactions.[249, 250, 252]

It has also been reported that the photo–catalytic production rate of H_2 can be significantly improved in the presence of alcohol, which provides suitable electron donors (also known as sacrificial agent/reagent).[258-260] Barreca *et al.* have successfully demonstrated excellent performance of Cu_2O photo–catalysis for generating H_2 in the presence of methanol.[13] They have suggested that methanol inhibits electron–hole recombination and acts partially as a hydrogen source.[13] However, efficient photo–catalytic activity of CuO for H_2 production has not been reported. This is despite that fact that the band gap of CuO is 1.2 eV, which makes CuO an efficient material to absorb sunlight. However, the position of the conduction band level limits its activity. Therefore, introducing a sacrificial agent is crucial to enable it to be used as a photo−catalyst. For example, Yao *et al.* have reported that CuO exhibits high photo−catalytic activity in oxalic acid solutions.[253] Oxalic acid, which is a common pollutant in industrial wastewater, is a strong reductive agent and acts as an electron donor.[261, 262]

4.3 Antimicrobial Applications

The antimicrobial properties of Cu_xO, in particular CuO, have attracted growing research interest. Nanostructured Cu_xO commonly offers a strong degree of chemical and physical stability. Most bacterial cells have cellular membranes that contain pores in the nanometer range. Cu_xO, with dimensions less than 20 nm, have shown antibacterial properties.[11, 263] The antimicrobial activity of CuO has been attributed to the production of reactive oxygen species (ROS) such as $^{\bullet}O_2^-$, $^{\bullet}HO_2$, $^{\bullet}OH$ and H_2O_2 which can also occur without exposure to any visible light owing to the small band gap of CuO.[264, 265] The generated ROS interact with outer cell walls to generate free radicals. The radicals penetrate into the inner cell membranes which lead to the disruption of the internal contents of the cell.[264, 265] The effectiveness of the antimicrobial agent appears to be related to the nature of the cell wall structures.[263, 265-267] *S. aureus* is composed of multiple layers of peptidoglycan with numerous pores, which are suggested to be more susceptible to intracellular transductions. In contrast, the cell walls of *E. coli* are relatively thin, mainly consisting of peptidoglycan and outer layers of lipopolysaccharide, lipoprotein and phospholipids, which are less prone to being attacked by CuO nanoparticles. As a result, nanostructured CuO has a higher antimicrobial activity against *S. aureus* than *E. coli.*[263, 264]

It has been demonstrated that nanostructured CuO antimicrobial activity can be enhanced by exposing it to light.[11, 264, 268-270] As described in section 4.2, light irradiation generates excited electron–hole pairs in the CuO and deactivation of the bacteria is possible *via* a photo–catalytic process.[11, 268] Akhavan *et al.* have reported an improvement of 22% of CuO antibacterial activity under illumination.[11]

4.4 Electrochemical Applications

The electrochemical properties of nanostructured Cu_xO as electrodes for lithium ion batteries (LIB) have also been of growing research interest. Cu_xO has many attractive advantages over conventional materials including high theoretical capacity (>600 and >350 $mAhg^{-1}$ for CuO and Cu_2O, respectively) and low cost.[271-273] One of the major issues with the use of Cu_xO in LIBs is its large volume variation during the Li^+ ion insertion/extraction processes, which leads to severe mechanical strains and a rapid decay in capacity.[271] Recently, there have been various reports demonstrating LIBs with high reversible capacity and cycling stability by synthesising Cu_xO/graphene nanocomposites.[271, 274, 275] Mai *et al.* reported an excellent reversible capacity of 583.5 $mAhg^{-1}$ with high cycling stability by incorporating CuO nanoparticles (~30 nm) onto graphene sheets (Figure 12a). The graphene sheets serve as a conductive network for fast electron transfer as well as buffered spaces to accommodate the CuO volume expansion/contraction during Li^+ insertion/extraction process.[274]

Nanostructuring Cu_xO into hollow nano/microstructures such as spheres, cubes or urchin–like structures increases its LIB performance.[201, 275-277] For example, Park *et al.* have successfully demonstrated that hollow CuO urchin–like nanoparticles possess a charge capacity above 560 $mAhg^{-1}$ (Figure 12b).[276] Wei *et al.* have discussed and listed three main advantages of hollow structures as anode materials for LIBs.[277] Zhou *et al.* have reported excellent LIB performance by integrating hollow nanostructures of CuO with graphene.[275] The composites exhibited a durable lifetime with reversible capacities as large as 640 $mAhg^{-1}$ (Figure 12c).[275]

4.5 Electrochromic Devices

Nanostructured Cu_2O electrochromic based systems, such as smart windows and optical displays, have been studied since the 1990s.[130] It has been found that Cu_2O exhibits cathodic electrochromism, being transparent under visible illumination in their oxidized state and almost black when switched to their reduced state in the presence of an electrolyte containing positive ions such as H^+, Li^+ and Na^+.[130, 278-281] Generally, it has

been found that the electrochromic process corresponds to the conversion of Cu_2O (transparent) to CuO (black) in a reversible reduction–oxidation process (redox).[278, 281] To date, the best coloration efficiency obtained by Cu_2O nanostructures has been up to 37 cm^2C^{-1}, which is only one–fourth of the best of those made from WO_3 nanoporous (141.5 cm^2C^{-1}).[278, 282] Unfortunately, nanostructured Cu_2O requires high coloration voltage and shows poor stability[279], and further work should be carried out to solve such important issues.

4.6 Sensing Applications

Cu_xO offers great potential for the development of highly sensitive, yet low cost sensors. This includes optical, gas and bio sensors. Photodetectors are important devices that can be used in various applications, including thermal imaging systems, free-space communications, navigator aids and ozone-layer monitoring.[283, 284] Among the semiconductor materials, Cu_xO has proven an attractive material for making photodetectors due to its relatively low band gap and remarkable optoelectronics properties.[70, 284-287]

Sahoo *et al.* have demonstrated excellent performance of photodetector based on Cu_2O nanowires.[285] They adopted metal-semiconductor-metal (MSM) technique for photon sensing under dark and illumination conditions. Figure 13(a-d) illustrated SEM micrographs of four such MSM devices with channel lengths (i.e. spacing between the electrodes) of 210, 260, 580 and 720 nm, respectively.[285] They observed that the channel length significantly influenced the photocurrent and bias dependence of the photo-to-dark-current ratio (Figure 13(e-h)).[285] Liao *et al.* reported the photoconductivity of Cu_2O nanowires measured under dark and blue (488 nm) laser illumination and the conductance of nanowires increased from 0.7 to 4.3 μ*S* under illumination. Remarkably, the photoconductivity response time was less than three seconds with good reversibility and stability.[70] CuO has also been extensively used in photodetector applications under visible and IR illumination (due to its relatively low band gap).[284, 286-288] Recent comprehensive reviews on the usage of CuO in photodetection are found elsewhere.[1]

Cu_xO also offers a great possibility for developing highly sensitive semiconductor-based gas sensors. The sensing properties of Cu_xO can be improved by decreasing its size to nanoscale dimensions (comparable to twice of the Debye length) and by adding appropriate dopants.[126, 289] Catalytic nanoparticles such as Pd,[290] Pt,[291] Ag[292] and Au[291, 293, 294] attached to the Cu_xO surface, further increases its sensitivity, mainly due to spill−over effects.[289] Cu_xO thin films have been demonstrated to be highly sensitive towards various gas species including C_2H_5OH,[14, 126, 294-298] CO,[296, 299, 300] NO_2[14, 300] and H_2S[53, 290, 301] (Figure 14).

The ability to tune the shape and dimensions of Cu_xO thereby creating superior chemical and physical properties can be exploited for chemosensors and biosensors. They also show unique surface chemistry, thermal and electrical properties and high surface-to-volume ratio which enhance the sensitivity and response of electrochemical sensors.[302]

Cu_xO has been used as a working electrode in electrochemical based biosensors including in glucose sensors.[303] Most electrochemical glucose sensors involve the use of the enzyme glucose oxidase. However, the greatest drawback of enzymatic sensors is their lack of stability due to the intrinsic nature of enzymes.[304, 305] Development of non-enzymatic sensors, using Cu_xO as the working electrode, has been reported.[305-307] Though non-enzymatic sensors are, by design, quite selective, CuO-based glucose sensors have a fast response times, possess a high degree of repeatability and are extremely stable.[303]

4.7 Tribology and Heat Transfer Applications

A large number of studies have reported that adding metal oxides such as Cu_xO in the form of nanoparticles to lubricants is an effective means to reduce wear and friction.[12, 80, 308-310] The friction–reduction and anti–wear behaviours are dependent on the characteristics of the nanoparticles including size (mostly in the range of 2 – 120 nm), morphology and concentration.[12] The colloidal effect, rolling friction effect, third body generation with nanomaterials and protective thin films formation mechanism have been proposed to justify the role of nanomaterials' anti–wear and friction–reduction properties.[80]

Wu *et al.* have compared the tribological properties of two lubricating oils (API–SF engine oil and Base oil) with CuO, TiO_2 and diamond nanoparticles used as additives. They found that CuO suspensions showed the highest reduction of friction coefficient (due to viscosity and rolling effect) and worn scar depth (owing to reduction of shearing stress) as compared to standard oils without nanoparticles.[12] The shapes of nanoparticles such as sphere, rods, sheets and wires play crucial roles in tribology in monitoring the friction and anti–wear properties. Recently, Gausian *et al.* have revealed that lubricity enhancement is attributed to the synergistic effect of uninterrupted supplies of CuO nanorods under contact surfaces and their rolling mechanism.[80]

In addition to the enhancement of tribological properties, nanofluids with dispersed Cu_xO nanoparticles have great potential for improving heat transfer especially in improving the efficiency of chillers, refrigerators and air–conditioners.[81, 310, 311] Many studies have reported that mixtures with suspended CuO nanoparticles have higher thermal conductivity than the conventional host fluid.[81] This is due to the thermal conductivity of CuO (76.5 W mK^{-1} which is much higher than ethylene glycol that has a value of 0.26 W mK^{-1}). Lee *at al.* have compared the thermal conductivity of CuO and Al_2O_3 nanoparticles suspended in ethylene glycol and found that the thermal conductivity of the CuO suspensions is 7% higher than the Al_2O_3 system.[312]

4.8 Field Emission Applications

The field emission (FE) properties of Cu_xO are far less reported than other oxides materials such as ZnO, SnO_2 and In_2O_3. Due to its relatively narrow band gap, nanostructured Cu_xO offers an attractive alternative to serve as a FE emitter.[313-315] In a FE system the emitting capability is believed to be highly dependent on both the properties of the material and configuration of the cathode.[34] It is known that materials with higher aspect ratios and sharp edges generally produce higher FE currents.[55, 313, 315] Zhu *et al.* have reported FE measurements of CuO nanowire films with a low turn−on field of 3.5−4.5 V μm^{-1}. They obtained a large current density of 0.45 mA cm^{-2} at an applied electric field of 7 V μm^{-1}.[314] Nanostructured Cu_2O also exhibits relatively high FE performance. Shi *et al.* have demonstrated Cu_2O micro−porous cubes with a low turn−on field of 3.1 V μm^{-1}. They showed a high current density of

1 mA cm^{-2} at an applied electric field of 11 V μm^{-1}.[55] It has also been reported that Cu_2O can be coupled with other metal oxides such as ZnO or TiO_2 to enhance its FE performance (Figure 15).[315-317] This enhanced FE is attributed to the alteration in electron affinity of Cu_xO by the other metal oxides forming a nano−heterojunction.[317] Additionally, the presence of the heterojunctions promotes charge separation, where the electrons move to ZnO or TiO_2 and the holes move to Cu_2O, which reduces the recombination of electron−hole pairs.[317]

4.9 Other Applications

Nanostructured Cu_xO has also been reported for many applications other than those presented in sections 4.1 to 4.8. Of note, nanostructured CuO has been used in ceramic resistors[318] and supercapacitors.[319, 320] Nanostructured Cu_2O has also been incorporated in memristors,[321-323] heterogeneous catalysis,[324-328] anti−fouling[329-331] and thin−film transistors.[2, 332, 333] Of course, there are other applications for which Cu_xO has been used, but these are beyond the scope of this review paper.

5. CONCLUSIONS AND FUTURE OUTLOOK

In this article, we have presented a comprehensive review of nanostructured Cu_xO focusing on their properties, preparation, processing and device applications. An overview of the material properties, including crystal structures, electronic band structures, optical, vibrational, electrical, thermal and magnetic as well as superconductivity were presented. The effect of doping on the band gap and the enhancement in electrical properties was also detailed. Though much effort has been channeled in producing *n*–type Cu_xO, the reproducibility and quality issues of the generated films are still questionable. This is potentially due to strong self-compensation effects and dopants solubility issues when *n*–type dopants are involved. Clearly, this issue must be overcome before high efficiency photovoltaic devices, based on homojunction Cu_2O devices will be realized.

Numerous synthesis techniques were reviewed, focusing on methods that produce nanostructured Cu_xO. Different synthesis techniques provide flexibility within the constraints of any particular applications needs. Therefore, it is essential that exploration of nanostructures Cu_xO synthesis continues and more innovative and low-cost routes are found in order to improve the future of the nanostructured Cu_xO and its many applications.

Additionally, we have discussed the major applications of nanostructured Cu_xO including optics, sensing, tribology, refrigeration, electrochemistry, photocatalysis, High–T_C superconductivity, electrochromics and antimicrobial devices. Due to the versatility of nanostructured Cu_xO, many more applications can be explored and are yet to be investigated.

To date, the majority of work in the area of Cu_xO has been devoted to CuO and Cu_2O, whilst the numbers of reports on Cu_4O_3 are significantly lower. Despite the fact that there is a very limited number of reports available, the authors believe that the study of nanostructured Cu_4O_3 might provide possible new materials insights and unique opportunities for incorporation into a wide-range of applications. Like to other copper oxides, nanostructured Cu_4O_3 has the potential to be used in tribology and heat transfer applications as well as antimicrobial devices. As with the other copper oxide structures, the potential gains from developing a low-cost, nanostructured material, like Cu_4O_3 for any of these applications is extremely enticing and expected to be explored.

Notes and references

[a]School of Electrical and Computer Engineering, RMIT University, Melbourne, VIC 3001, Australia
[b]Faculty of Electrical Engineering, Universiti Teknologi MARA, 40450 Shah Alam, Malaysia
[c]Freie Universität Berlin, Fachbereich Physik, 14195 Berlin, Germany
[d]School of Chemistry, Physics and Mechanical Engineering, Queensland University of Technology, GPO Box 2434, Brisbane, QLD, 4001, Australia

1. Q. Zhang, K. Zhang, D. Xu, G. Yang, H. Huang, F. Nie, C. Liu and S. Yang, *Prog. Mater. Sci.*, 2014, **60**, 208-337.
2. B. K. Meyer, A. Polity, D. Reppin, M. Becker, P. Hering, P. J. Klar, T. Sander, C. Reindl, J. Benz, M. Eickhoff, C. Heiliger, M. Heinemann, J. Blaesing, A. Krost, S. Shokovets, C. Mueller and C. Ronning, *Phys. Status Solidi B*, 2012, **249**, 1487-1509.
3. K. P. Musselman, A. Marin, L. Schmidt-Mende and J. L. MacManus-Driscoll, *Adv. Funct. Mater.*, 2012, **22**, 2202-2208.
4. V. Gedzevičiūtė, N. Welter, U. Schüssler and C. Weiss, *Archaeol. Anthropol. Sci.*, 2009, **1**, 15-29.
5. P. Colomban, G. Sagon and X. Faurel, *J. Raman Spectrosc.*, 2001, **32**, 351-360.
6. P. E. Russell, *J. Agr. Sci.*, 2005, **143**, 11-25.
7. E. Somers, *J. Sci. Food Agr.*, 1956, **7**, 160-172.
8. I. Omae, *Chem. rev.*, 2003, **103**, 3431-3448.
9. M. Srinivasan and G. Swain, *Environ. Manage.*, 2007, **39**, 423-441.
10. K. P. Musselman, A. Marin, A. Wisnet, C. Scheu, J. L. MacManus-Driscoll and L. Schmidt-Mende, *Adv. Funct. Mater.*, 2011, **21**, 573-582.
11. O. Akhavan and E. Ghaderi, *Surf. Coat. Tech.*, 2010, **205**, 219-223.
12. Y. Y. Wu, W. C. Tsui and T. C. Liu, *Wear*, 2007, **262**, 819-825.
13. D. Barreca, P. Fornasiero, A. Gasparotto, V. Gombac, C. Maccato, T. Montini and E. Tondello, *Chemsuschem*, 2009, **2**, 230-233.
14. D. D. Li, J. Hu, R. Q. Wu and J. G. Lu, *Nanotechnology*, 2010, **21**.
15. T. Ito, H. Yamaguchi, K. Okabe and T. Masumi, *J. Mater. Sci.*, 1998, **33**, 3555-3566.
16. W. Y. Ching, Y. N. Xu and K. W. Wong, *Phys. Rev. B*, 1989, **40**, 7684-7695.
17. S. Sun and Z. Yang, *RSC Adv.*, 2014, **4**, 3804-3822.
18. S. Asbrink and L. J. Norrby, *Acta Crystall. B-Stru.*, 1970, **B 26**, 8-&.
19. M. Heinemann, B. Eifert and C. Heiliger, *Phys. Rev. B*, 2013, **87**.
20. J. F. Pierson, E. Duverger and O. Banakh, *J. Solid State Chem.*, 2007, **180**, 968-973.
21. M. Okeeffe and J. O. Bovin, *Am. Mineral.*, 1978, **63**, 180-185.
22. C. Frondel, *Am. Mineral.*, 1941, **26**, 657-672.
23. A. E. Rakhshani and F. K. Barakat, *Mater. Lett.*, 1987, **6**, 37-40.
24. M. T. S. Nair, L. Guerrero, O. L. Arenas and P. K. Nair, *Appl. Surf. Sci.*, 1999, **150**, 143-151.
25. M. F. Al-Kuhaili, *Vacuum*, 2008, **82**, 623-629.
26. A. Chen, G. Yang, H. Long, F. Li, Y. Li and P. Lu, *Thin Solid Films*, 2009, **517**, 4277-4280.
27. J. Ghijsen, L. H. Tjeng, J. Vanelp, H. Eskes, J. Westerink, G. A. Sawatzky and M. T. Czyzyk, *Phys. Rev. B*, 1988, **38**, 11322-11330.
28. A. A. Ogwu, E. Bouquerel, O. Ademosu, S. Moh, E. Crossan and F. Placido, *J. Phys. D Appl. Phys.*, 2005, **38**, 266-271.
29. M. Izaki, *Thin Solid Films*, 2012, **520**, 2434-2437.
30. K. Nakaoka, J. Ueyama and K. Ogura, *J. Electrochem. Soc.*, 2004, **151**, C661-C665.
31. J. C. Tauc, *Optical Properties of Solids*, North-Holland, Amsterdam, 1972.

32. J. F. Pierson, A. Thobor-Keck and A. Billard, *Appl. Surf. Sci.*, 2003, **210**, 359-367.
33. S. Rehman, A. Mumtaz and S. K. Hasanain, *J. Nanopart. Res.*, 2011, **13**, 2497-2507.
34. H. D. Zheng, J. Z. Ou, M. S. Strano, R. B. Kaner, A. Mitchell and K. Kalantar-Zadeh, *Adv. Funct. Mater.*, 2011, **21**, 2175-2196.
35. A. D. Yoffe, *Adv. Phys.*, 1993, **42**, 173-266.
36. M. Yang and J. He, *J. Colloid Interf. Sci.*, 2011, **355**, 15-22.
37. J. Liu, X. Huang, Y. Li, K. M. Sulieman, X. He and F. Sun, *J. Mater. Chem.*, 2006, **16**, 4427-4434.
38. A. Shui, W. Zhu, L. Xu, D. Qin and Y. Wang, *Ceram. Int.*, 2013, **39**, 8715-8722.
39. Y. Gulen, F. Bayansal, B. Sahin, H. A. Cetinkara and H. S. Guder, *Ceram. Int.*, 2013, **39**, 6475-6480.
40. N. M. Basith, J. J. Vijaya, L. J. Kennedy, M. Bououdina and S. Hussain, *J. Nanosci. Nanotechno.*, 2014, **14**, 2577-2583.
41. N. M. Basith, J. J. Vijaya, L. J. Kennedy and M. Bououdina, *Mat. Sci. Semicon. Proc.*, 2014, **17**, 110-118.
42. Y. Peng, Z. Zhang, P. Thien Viet, Y. Zhao, P. Wu and J. Wang, *J. Appl. Phys.*, 2012, **111**.
43. L. Y. Isseroff and E. A. Carter, *Chem. Mater.*, 2013, **25**, 253-265.
44. Y. Chang, J. J. Teo and H. C. Zeng, *Langmuir*, 2005, **21**, 1074-1079.
45. B. Balamurugan and B. R. Mehta, *Thin Solid Films*, 2001, **396**, 90-96.
46. P. Poulopoulos, S. Baskoutas, S. D. Pappas, C. S. Garoufalis, S. A. Droulias, A. Zamani and V. Kapaklis, *J. Phys. Chem. C*, 2011, **115**, 14839-14843.
47. A. Thobor and J. F. Pierson, *Mater. Lett.*, 2003, **57**, 3676-3680.
48. J. F. Pierson, D. Wiederkehr and A. Billard, *Thin Solid Films*, 2005, **478**, 196-205.
49. T. Ito, T. Kawashima, H. Yamaguchi, T. Masumi and S. Adachi, *J. Phys. Soc. Jpn.*, 1998, **67**, 2125-2131.
50. T. Ito, H. Yamaguchi, T. Masumi and S. Adachi, *J. Phys. Soc. Jpn.*, 1998, **67**, 3304-3309.
51. C. Malerba, F. Biccari, C. Leonor Azanza Ricardo, M. D'Incau, P. Scardi and A. Mittiga, *Sol. Energ. Mat. Sol. C.*, 2011, **95**, 2848-2854.
52. K. Borgohain, N. Murase and S. Mahamuni, *J. Appl. Phys.*, 2002, **92**, 1292-1297.
53. J. T. Zhang, J. F. Liu, Q. Peng, X. Wang and Y. D. Li, *Chem. Mater.*, 2006, **18**, 867-871.
54. H.-H. Lin, C.-Y. Wang, H. C. Shih, J.-M. Chen and C.-T. Hsieh, *J. Appl. Phys.*, 2004, **95**, 5889-5895.
55. H. Shi, K. Yu, F. Sun and Z. Zhu, *CrystEngComm*, 2012, **14**, 278-285.
56. H. Shi, K. Yu, Y. Wang, Q. Wang and Z. Zhu, *Appl. Phys. A-Mater.*, 2012, **108**, 709-717.
57. M. M. Beg and S. M. Shapiro, *Phys. Rev. B*, 1976, **13**, 1728-1734.
58. M. Ivanda, D. Waasmaier, A. Endriss, J. Ihringer, A. Kirfel and W. Kiefer, *J. Raman Spectrosc.*, 1997, **28**, 487-493.
59. R. Mittal, S. L. Chaplot, S. K. Mishra and P. P. Bose, *Phys. Rev. B*, 2007, **75**.
60. W. Reichardt, F. Gompf, M. Ain and B. M. Wanklyn, *Z. Phys. B Con. Mat.*, 1990, **81**, 19-24.
61. L. Debbichi, M. C. M. de Lucas, J. F. Pierson and P. Kruger, *J. Phys. Chem. C*, 2012, **116**, 10232-10237.
62. P. H. Shih, C. L. Cheng and S. Y. Wu, *Nanoscale Res. Lett.*, 2013, **8**.
63. R. J. Elliott, *Phys. Rev.*, 1961, **124**, 340-&.
64. Y. K. Jeong and G. M. Choi, *J. Phys. Chem. Solids*, 1996, **57**, 81-84.
65. A. P. Young and C. M. Schwartz, *J. Phys. Chem. Solids*, 1969, **30**, 249-252.
66. S. Suda, S. Fujitsu, K. Koumoto and H. Yanagida, *Jpn. J. Appl. Phys. 1*, 1992, **31**, 2488-2491.
67. D. Gopalakrishna, K. Vijayalakshmi and C. Ravidhas, *Ceram. Int.*, 2013, **39**, 7685-7691.
68. Y. Ohya, S. Ito, T. Ban and Y. Takahashi, in *Key. eng. mat.*, eds. N. Murata, K. Shinozaki and T. Kimura, 2000, pp. 113-116.
69. P. Shao, S. Deng, J. Chen, J. Chen and N. Xu, *J. Appl. Phys.*, 2011, **109**.
70. L. Liao, B. Yan, Y. F. Hao, G. Z. Xing, J. P. Liu, B. C. Zhao, Z. X. Shen, T. Wu, L. Wang, J. T. L. Thong, C. M. Li, W. Huang and T. Yu, *Appl. Phys. Lett.*, 2009, **94**.
71. Y. W. Tan, X. Y. Xue, Q. Peng, H. Zhao, T. H. Wang and Y. D. Li, *Nano Lett.*, 2007, **7**, 3723-3728.
72. S. Ishizuka and K. Akimoto, *Appl. Phys. Lett.*, 2004, **85**, 4920-4922.
73. K. Mizuno, M. Izaki, K. Murase, T. Shinagawa, M. Chigane, M. Inaba, A. Tasaka and Y. Awakura, *J. Electrochem. Soc.*, 2005, **152**, C179-C182.
74. P. Thien Viet, M. Rao, P. Andreasson, Y. Peng, J. Wang and K. B. Jinesh, *Appl. Phys. Lett.*, 2013, **102**.
75. D. O. Scanlon and G. W. Watson, *J. Phys. Chem. Lett.*, 2010, **1**, 2582-2585.
76. L. Q. Wang and J. Fan, *Nanoscale Res. Lett.*, 2010, **5**, 1241-1252.
77. X. Wei, H. Zhu, T. Kong and L. Wang, *Int. J. Heat Mass Tran.*, 2009, **52**, 4371-4374.
78. Y. J. Hwang, Y. C. Ahn, H. S. Shin, C. G. Lee, G. T. Kim, H. S. Park and J. K. Lee, *Curr. Appl. Phys.*, 2006, **6**, 1068-1071.
79. S. Walia, S. Balendhran, H. Nili, S. Zhuiykov, G. Rosengarten, Q. H. Wang, M. Bhaskaran, S. Sriram, M. S. Strano and K. Kalantar-zadeh, *Prog. Mater. Sci.*, 2013, **58**, 1443-1489.
80. R. Gusain and O. P. Khatri, *J. Mater. Chem. A*, 2013, **1**, 5612-5619.
81. R. Saidur, S. N. Kazi, M. S. Hossain, M. M. Rahman and H. A. Mohammed, *Renew. Sust. Energ. Rev.*, 2011, **15**, 310-323.
82. H. Timm and J. Janek, *Solid State Ionics*, 2005, **176**, 1131-1143.
83. X. Chen, D. Parker, M. H. Du and D. J. Singh, *New J. Phys.*, 2013, **15**.
84. H. A. Mintsa, G. Roy, C. T. Nguyen and D. Doucet, *Int. J. Therm. Sci.*, 2009, **48**, 363-371.
85. C. H. Li and G. P. Peterson, *J. Appl. Phys.*, 2006, **99**.
86. M. J. Nine, B. Munkhbayar, M. S. Rahman, H. Chung and H. Jeong, *Mater. Chem. Phys.*, 2013, **141**, 636-642.
87. H. Zhu, D. Han, Z. Meng, D. Wu and C. Zhang, *Nanoscale Res. Lett.*, 2011, **6**.
88. P. A. Korzhavyi, I. L. Soroka, E. I. Isaev, C. Lilja and B. Johansson, *P. Natl. Acad. Sci. USA*, 2012, **109**, 686-689.
89. J. Leitner, D. Sedmidubský, B. Doušová, A. Strejc and M. Nevřiva, *Thermochim. Acta*, 2000, **348**, 49-51.
90. M. W. Chase, C. A. Davies, J. R. Downey, D. J. Frurip, R. A. McDonald and A. N. Syverud, *J. Phys. Chem. Ref. Data*, 1985, **14**, 1-926.
91. E. Gmelin, *Indian J. Pure Ap. Phys.*, 1992, **30**, 596-608.
92. L. V. Gregor, *J. Phys. Chem.*, 1962, **66**, 1645-&.
93. J. H. Hu and H. L. Johnston, *J. Am. Chem. Soc.*, 1951, **73**, 4550-4551.
94. D. D. Lawrie, J. P. Franck and C.-T. Lin, *Physica C*, 1998, **297**, 59-63.
95. L. Pinsard-Gaudart, J. Rodriguez-Carvajal, A. Gukasov and P. Monod, *Phys. Rev. B*, 2004, **69**.
96. M. H. Whangbo and H. J. Koo, *Inorg. Chem.*, 2002, **41**, 3570-3577.
97. B. X. Yang, J. M. Tranquada and G. Shirane, *Phys. Rev. B*, 1988, **38**, 174-178.
98. B. X. Yang, J. M. Tranquada and G. Shirane, *Phys. Rev. B*, 1988, **38**, 174-178.
99. P. J. Brown, T. Chattopadhyay, J. B. Forsyth, V. Nunez and F. Tasset, *J. Phys.-Condens.Mat.*, 1991, **3**, 4281-4287.
100. M. S. Seehra and A. Punnoose, *Solid State Commun.*, 2003, **128**, 299-302.
101. X. G. Zheng, T. Mori, K. Nishiyama, W. Higemoto and C. N. Xu, *Solid State Commun.*, 2004, **132**, 493-496.
102. A. Punnoose, H. Magnone, M. S. Seehra and J. Bonevich, *Phys. Rev. B*, 2001, **64**.
103. D. Shang, K. Yu, Y. Zhang, J. Xu, J. Wu, Y. e. Xu, L. Li and Z. Zhu, *Appl. Surf. Sci.*, 2009, **255**, 4093-4096.
104. D. Gao, G. Yang, J. Li, J. Zhang, J. Zhang and D. Xue, *J. Phys. Chem. C*, 2010, **114**, 18347-18351.
105. D. Gao, J. Zhang, J. Zhu, J. Qi, Z. Zhang, W. Sui, H. Shi and D. Xue, *Nanoscale Res. Lett.*, 2010, **5**, 769-772.
106. S. H. Pan, J. P. O'Neal, R. L. Badzey, C. Chamon, H. Ding, J. R. Engelbrecht, Z. Wang, H. Eisaki, S. Uchida, A. K. Guptak, K. W.

Ng, E. W. Hudson, K. M. Lang and J. C. Davis, *Nature*, 2001, **413**, 282-285.
107. M. A. Kastner, R. J. Birgeneau, G. Shirane and Y. Endoh, *Rev. Mod. Phys.*, 1998, **70**, 897-928.
108. J. M. Tranquada, H. Woo, T. G. Perring, H. Goka, G. D. Gu, G. Xu, M. Fujita and K. Yamada, *Nature*, 2004, **429**, 534-538.
109. M. Karppinen and H. Yamauchi, *Philos. Mag. B*, 1999, **79**, 343-366.
110. H. Yamauchi and M. Karppinen, *Mat. Sci. Eng. B-Solid*, 1998, **54**, 92-97.
111. X. Han, K. Han and M. Tao, *Electrochem. Solid Lett.*, 2009, **12**, H89-H91.
112. K. Han and M. Tao, in *Photovoltaics for the 21st Century 5*, eds. M. Tao, P. Chang, K. Kakimoto, M. Sunkara, J. Brownson, C. Claeys, K. Rajeshwar and D. Yang, 2010, pp. 103-109.
113. X. Han, K. Han and M. Tao, *Thin Solid Films*, 2010, **518**, 5363-5367.
114. C. A. N. Fernando and S. K. Wetthasinghe, *Sol. Energ. Mat. Sol. C.*, 2000, **63**, 299-308.
115. Y. Okamoto, S. Ishizuka, S. Kato, T. Sakurai, N. Fujiwara, H. Kobayashi and K. Akimoto, *Appl. Phys. Lett.*, 2003, **82**, 1060-1062.
116. B. B. Li, L. Lin, H. L. Shen, F. E. Boafo, Z. F. Chen, B. Liu and R. Zhang, *Eur. Phys. J-Appl. Phys.*, 2012, **58**.
117. K. Akimoto, S. Ishizuka, M. Yanagita, Y. Nawa, G. K. Paul and T. Sakurai, *Sol. Energy*, 2006, ***80***, 715-722.
118. S. Ishizuka, S. Kato, Y. Okamoto and K. Akimoto, *Appl. Phys. Lett.*, 2002, **80**, 950-952.
119. S. Ishizuka, S. Kato, Y. Okamoto and K. Akimoto, *J. Cryst. Growth*, 2002, **237–239, Part 1**, 616-620.
120. C. L. Chu, H. C. Lu, C. Y. Lo, C. Y. Lai and Y. H. Wang, *Physica B*, 2009, **404**, 4831-4834.
121. H.-C. Lu, C.-L. Chu, C.-Y. Lai and Y.-H. Wang, *Thin Solid Films*, 2009, **517**, 4408-4412.
122. A. S. Reddy, H.-H. Park, V. S. Reddy, K. V. S. Reddy, N. S. Sarma, S. Kaleemulla, S. Uthanna and P. S. Reddy, *Mater. Chem. Phys.*, 2008, **110**, 397-401.
123. H. Zhu, J. Zhang, C. Li, F. Pan, T. Wang and B. Huang, *Thin Solid Films*, 2009, **517**, 5700-5704.
124. A. R. Rastkar, A. R. Niknam and B. Shokri, *Thin Solid Films*, 2009, **517**, 5464-5467.
125. N. G. Elfadill, M. R. Hashim, K. M. Chahrour, M. A. Qaeed and C. Wang, *J. Mater. Sci.-Mater. El.*, 2014, **25**, 262-266.
126. A. S. Zoolfakar, M. Z. Ahmad, R. A. Rani, J. Z. Ou, S. Balendhran, S. Zhuiykov, K. Latham, W. Wlodarski and K. Kalantar-zadeh, *Sens. Actuator B Chem.*, 2013, **185**, 620-627.
127. K. J. Blobaum, D. Van Heerden, A. J. Wagner, D. H. Fairbrother and T. P. Weihs, *J. Mater. Res.*, 2003, **18**, 1535-1542.
128. A. V. Richthofen, R. Domnick and R. Cremer, *Fresen. J. Anal. Chem.*, 1997, **358**, 312-315.
129. P. K. Ooi, S. S. Ng, M. J. Abdullah, H. Abu Hassan and Z. Hassan, *Mater. Chem. Phys.*, 2013, **140**, 243-248.
130. N. Özer and F. Tepehan, *Sol. Energ. Mat. Sol. C.*, 1993, **30**, 13-26.
131. K. Santra, C. K. Sarkar, M. K. Mukherjee and B. Ghosh, *Thin Solid Films*, 1992, **213**, 226-229.
132. B. Balamurugan, B. R. Mehta, D. K. Avasthi, F. Singh, A. K. Arora, M. Rajalakshmi, G. Raghavan, A. K. Tyagi and S. M. Shivaprasad, *J. Appl. Phys.*, 2002, **92**, 3304-3310.
133. V. A. Gevorkyan, A. E. Reymers, M. N. Nersesyan and M. A. Arzakantsyan, *J. Phys. Conf. Ser.*, 2012, **350**.
134. S. Kim, K. Hong, K. Kim, I. Lee and J.-L. Lee, *J. Mater. Chem.*, 2012, **22**, 2039-2044.
135. M. Vila, C. Diaz-Guerra and J. Piqueras, *J. Phys. D Appl. Phys.*, 2010, **43**.
136. M. Kaur, K. P. Muthe, S. K. Despande, S. Choudhury, J. B. Singh, N. Verma, S. K. Gupta and J. V. Yakhmi, *J. Cryst. Growth*, 2006, **289**, 670-675.
137. A. H. Jayatissa, K. Guo and A. C. Jayasuriya, *Appl. Surf. Sci.*, 2009, **255**, 9474-9479.
138. J. Liang, N. Kishi, T. Soga and T. Jimbo, *Appl. Surf. Sci.*, 2010, **257**, 62-66.
139. Y.-M. Juan, H.-T. Hsueh, T.-C. Cheng, C.-W. Wu and S.-J. Chang, *ECS Solid State Lett.*, 2014, **3**, P30-P32.
140. A. O. Musa, T. Akomolafe and M. J. Carter, *Sol. Energ. Mat. Sol. C.*, 1998, **51**, 305-316.
141. G. Filipic and U. Cvelbar, *Nanotechnology*, 2012, **23**.
142. Y. Yue, M. Chen, Y. Ju and L. Zhang, *Scripta Mater.*, 2012, **66**, 81-84.
143. L. D. Valladares, D. H. Salinas, A. B. Dominguez, D. A. Najarro, S. I. Khondaker, T. Mitrelias, C. H. W. Barnes, J. A. Aguiar and Y. Majima, *Thin Solid Films*, 2012, **520**, 6368-6374.
144. X. Jiang, T. Herricks and Y. Xia, *Nano Lett.*, 2002, **2**, 1333-1338.
145. L. S. Huang, S. G. Yang, T. Li, B. X. Gu, Y. W. Du, Y. N. Lu and S. Z. Shi, *J. Cryst. Growth*, 2004, **260**, 130-135.
146. F. Mumm and P. Sikorski, *Nanotechnology*, 2011, **22**.
147. K. L. Zhang, C. Rossi, C. Tenailleau, P. Alphonse and J. Y. Chane-Ching, *Nanotechnology*, 2007, **18**.
148. Q. Zhang, J. Wang, D. Xu, Z. Wang, X. Li and K. Zhang, *J. Mater. Chem. A*, 2014, **2**, 3865-3874.
149. Q. B. Zhang, D. Xu, T. F. Hung and K. Zhang, *Nanotechnology*, 2013, **24**.
150. R.-C. Wang and C.-H. Li, *Cryst. Growth Des.*, 2009, **9**, 2229-2234.
151. Q. Zhang, D. Xu, X. Zhou, X. Wu and K. Zhang, *Small*, 2014, **10**, 935-943.
152. H. T. Hsueh, T. J. Hsueh, S. J. Chang, F. Y. Hung, T. Y. Tsai, W. Y. Weng, C. L. Hsu and B. T. Dai, *Sens. Actuator B Chem.*, 2011, **156**, 906-911.
153. Y. Fu, H. Lei, X. Wang, D. Yan, L. Cao, G. Yao, C. Shen, L. Peng, Y. Zhao, Y. Wang and W. Wu, *Appl. Surf. Sci.*, 2013, **273**, 19-23.
154. A. Chen, H. Long, X. Li, Y. Li, G. Yang and P. Lu, *Vacuum*, 2009, **83**, 927-930.
155. M. Kawwam, F. Alharbi, A. Aldwayyan and K. Lebbou, *Appl. Surf. Sci.*, 2012, **258**, 9949-9953.
156. W. Seiler, E. Millon, J. Perrière, R. Benzerga and C. Boulmer-Leborgne, *J. Cryst. Growth*, 2009, **311**, 3352-3358.
157. M. Kawwam, F. H. Alharbi, T. Kayed, A. Aldwayyan, A. Alyamani, N. Tabet and K. Lebbou, *Appl. Surf. Sci.*, 2013, **276**, 7-12.
158. K. P. Muthe, J. C. Vyas, S. N. Narang, D. K. Aswal, S. K. Gupta, D. Bhattacharya, R. Pinto, G. P. Kothiyal and S. C. Sabharwal, *Thin Solid Films*, 1998, **324**, 37-43.
159. K. Kawaguchi, R. Kita, M. Nishiyama and T. Morishita, *J. Cryst. Growth*, 1994, **143**, 221-226.
160. J. Li, Z. Mei, D. Ye, H. Liang, Y. Liu and X. Du, *J. Cryst. Growth*, 2012, **353**, 63-67.
161. D. S. Darvish and H. A. Atwater, *J. Cryst. Growth*, 2011, **319**, 39-43.
162. J. Medina-Valtierra, C. Frausto-Reyes, G. Camarillo-Martinez and J. A. Ramirez-Ortiz, *J. A. Appl. Catal.*, 2009, **356**, 36-42.
163. J. Ramirez-Ortiza, T. Ogura, J. Medina-Valtierra, S. E. Acosta-Ortiz, P. Bosch, J. A. de los Reyes and V. H. Lara, *Appl. Surf. Sci.*, 2001, **174**, 177-184.
164. C. R. Crick and I. P. Parkin, *J. Mater. Chem.*, 2011, **21**, 14712-14716.
165. T. Kosugi and S. Kaneko, *J. Am. Ceram. Soc.*, 1998, **81**, 3117-3124.
166. J. Morales, L. Sanchez, F. Martin, J. R. Ramos-Barrado and M. Sanchez, *Electrochim. Acta*, 2004, **49**, 4589-4597.
167. G. Q. Jian, L. Liu and M. R. Zachariah, *Adv. Funct. Mater.*, 2013, **23**, 1341-1346.
168. T. Ghodselahi, M. A. Vesaghi, A. Shafiekhani, A. Baghizadeh and M. Lameii, *Appl. Surf. Sci.*, 2008, **255**, 2730-2734.
169. D. Barreca, A. Gasparotto, C. Maccato, E. Tondello, O. I. Lebedev and G. Van Tendeloo, *Cryst. Growth Des.*, 2009, **9**, 2470-2480.
170. F. Pola-Albores, W. Antunez-Flores, P. Amezaga-Madrid, E. Rios-Valdovinos, M. Valenzuela-Zapata, F. Paraguay-Delgado and M. Miki-Yoshida, *J. Cryst. Growth*, 2012, **351**, 77-82.
171. P. Pattanasattayavong, S. Thomas, G. Adamopoulos, M. A. McLachlan and T. D. Anthopoulos, *Appl. Phys. Lett.*, 2013, **102**.
172. O. Waser, M. Hess, A. Guentner, P. Novak and S. E. Pratsinis, *J. Power Sources*, 2013, **241**, 415-422.

173. A. S. Zoolfakar, R. A. Rani, A. J. Morfa, S. Balendhran, A. P. O'Mullane, S. Zhuiykov and K. Kalantar-zadeh, *J. Mater. Chem.*, 2012, **22**, 21767-21775.
174. M. Izaki, M. Nagai, K. Maeda, F. B. Mohamad, K. Motomura, J. Sasano, T. Shinagawa and S. Watase, *J. Electrochem. Soc.*, 2011, **158**, D578-D584.
175. M. Izaki, T. Shinagawa, K.-T. Mizuno, Y. Ida, M. Inaba and A. Tasaka, *J. Phys. D Appl. Phys.*, 2007, **40**, 3326-3329.
176. J. Sasano, K. Motomura, M. Nagai, F. B. Mohamad and M. Izaki, *Electrochemistry*, 2011, **79**, 831-837.
177. B. M. Fariza, J. Sasano, T. Shinagawa, S. Watase and M. Izaki, *Thin Solid Films*, 2012, **520**, 2261-2264.
178. B. M. Fariza, J. Sasano, T. Shinagawa, H. Nakano, S. Watase and M. Izaki, *J. Electrochem. Soc.*, 2011, **158**, 621-625.
179. J. B. Cui and U. J. Gibson, *J. Phys. Chem. B*, 2010, **114**, 6408-6412.
180. H. Wei, H. Gong, Y. Wang, X. Hu, L. Chen, H. Xu, P. Liu and B. Cao, *Crystengcomm*, 2011, **13**, 6065-6070.
181. P. Poizot, C. J. Hung, M. P. Nikiforov, E. W. Bohannan and J. A. Switzer, *Electrochem. Solid St.*, 2003, **6**, C21-C25.
182. W. Y. Zhao, W. Y. Fu, H. B. Yang, C. J. Tian, M. H. Li, Y. X. Li, L. N. Zhang, Y. M. Sui, X. M. Zhou, H. Chen and G. T. Zou, *Crystengcomm*, 2011, **13**, 2871-2877.
183. M. Xu, F. Wang, B. Ding, X. Song and J. Fang, *RSC Advances*, 2012, **2**, 2240-2243.
184. G. Q. Yuan, H. F. Jiang, C. Lin and S. J. Liao, *J. Cryst. Growth*, 2007, **303**, 400-406.
185. G. Yu, X. Hu, D. Liu, D. Sun, J. Li, H. Zhang, H. Liu and J. Wang, *J. Electroanal. Chem.*, 2010, **638**, 225-230.
186. H. Ju, J. K. Lee, J. Lee and J. Lee, *Curr. Appl. Phys.*, 2012, **12**, 60-64.
187. S. Bijani, R. Schrebler, E. A. Dalchiele, M. Gabas, L. Martinez and J. R. Ramos-Barrado, *J. Phys. Chem. C*, 2011, **115**, 21373-21382.
188. M. J. Siegfried and K.-S. Choi, *J. Am. Chem. Soc.*, 2006, **128**, 10356-10357.
189. M. J. Siegfried and K. S. Choi, *Angew. Chem. Int. Edit.*, 2005, **44**, 3218-3223.
190. S. Z. Li, H. Zhang, Y. J. Ji and D. R. Yang, *Nanotechnology*, 2004, **15**, 1428-1432.
191. X. Wang, G. Xi, S. Xiong, Y. Liu, B. Xi, W. Yu and Y. Qian, *Cryst. Growth Des*, 2007, **7**, 930-934.
192. M. H. Cao, C. W. Hu, Y. H. Wang, Y. H. Guo, C. X. Guo and E. B. Wang, *Chem. Commun.*, 2003, 1884-1885.
193. C. Yang, X. Su, F. Xiao, J. Jian and J. Wang, *Sens. Actuator B Chem.*, 2011, **158**, 299-303.
194. Z. H. Yang, J. Xu, W. X. Zhang, A. P. Liu and S. P. Tang, *J. Solid State Chem.*, 2007, **180**, 1390-1396.
195. L. Liu, K. Hong, T. Hu and M. Xu, *J. Alloy Comp.*, 2012, **511**, 195-197.
196. H. Yu, J. Yu, S. Liu and S. Mann, *Chem. Mater.*, 2007, **19**, 4327-4334.
197. Z. Z. Chen, E. W. Shi, Y. Q. Zheng, W. J. Li, B. Xiao and J. Y. Zhuang, *J. Cryst. Growth*, 2003, **249**, 294-300.
198. S. M. Gupta and M. Tripathi, *Cent. Eur. J. Chem.*, 2012, **10**, 279-294.
199. M. Rajamathi and R. Seshadri, *Curr. Opin. Solid St. M.*, 2002, **6**, 337-345.
200. G.-D. Yao, Z.-B. Huo and F.-M. Jin, *Res. Chem. Intermediat.*, 2011, **37**, 351-358.
201. L. Zhao, H. Chen, Y. Wang, H. Che, P. Gunawan, Z. Zhong, H. Li and F. Su, *Chem. Mater.*, 2012, **24**, 1136-1142.
202. A. Aslani and V. Oroojpour, *Physica B*, 2011, **406**, 144-149.
203. A. Aslani, *Physica B*, 2011, **406**, 150-154.
204. X.-Y. Yu, R.-X. Xu, C. Gao, T. Luo, Y. Jia, J.-H. Liu and X.-J. Huang, *ACS Appl. Mater. Interfaces*, 2012, **4**, 1954-1962.
205. S. J. Chen, X. T. Chen, Z. L. Xue, L. H. Li and X. Z. You, *J. Cryst. Growth*, 2002, **246**, 169-175.
206. J. W. Zhu, D. Li, H. Q. Chen, X. J. Yang, L. Lu and X. Wang, *Mater. Lett*, 2004, **58**, 3324-3327.
207. R. Wu, Z. Ma, Z. Gu and Y. Yang, *J. Alloy. Compd.*, 2010, **504**, 45-49.
208. C. H. Lu, L. M. Qi, J. H. Yang, D. Y. Zhang, N. Z. Wu and J. M. Ma, *J. Phys. Chem. B*, 2004, **108**, 17825-17831.
209. W. Wang, L. Wang, H. Shi and Y. Liang, *Crystengcomm*, 2012, **14**, 5914-5922.
210. K. Chen and D. Xue, *J. Phys. Chem. C*, 2013, **117**, 22576-22583.
211. Z. Yang, J. Xu, W. Zhang, A. Liu and S. Tang, *J. Solid State Chem.*, 2007, **180**, 1390-1396.
212. J. Huang, Y. Dai, C. Gu, Y. Sun and J. Liu, *J. Alloy. Compd.*, 2013, **575**, 115-122.
213. H. Zhang, J. Feng and M. Zhang, *Mater. Res. Bull.*, 2008, **43**, 3221-3226.
214. C. Xia, X. Cai, W. Ning and G. Lin, *Anal. Chim. Acta*, 2011, **691**, 43-47.
215. L. Zheng and X. Liu, *Mater. Lett.*, 2007, **61**, 2222-2226.
216. Y. Xu, D. Chen, M. Jiao and K. Xue, *Mater. Res. Bull.*, 2007, **42**, 1723-1731.
217. L. F. Gou and C. J. Murphy, *Nano Lett.*, 2003, **3**, 231-234.
218. M. Yin, C. K. Wu, Y. B. Lou, C. Burda, J. T. Koberstein, Y. M. Zhu and S. O'Brien, *J. Am. Chem. Soc.*, 2005, **127**, 9506-9511.
219. L. Gou and C. J. Murphy, *J. Mater. Chem.*, 2004, **14**, 735-738.
220. M. D. Susman, Y. Feldman, A. Vaskevich and I. Rubinstein, *ACS Nano*, 2014, **8**, 162-174.
221. C.-H. Kuo and M. H. Huang, *J. Phys. Chem. C*, 2008, **112**, 18355-18360.
222. J.-Y. Ho and M. H. Huang, *J. Phys. Chem. C*, 2009, **113**, 14159-14164.
223. H. Xu, W. Wang and W. Zhu, *J. Phys. Chem. B*, 2006, **110**, 13829-13834.
224. W. Z. Wang, G. H. Wang, X. S. Wang, Y. J. Zhan, Y. K. Liu and C. L. Zheng, *Adv. Mater.*, 2002, **14**, 67-69.
225. L. Armelao, D. Barreca, M. Bertapelle, G. Bottaro, C. Sada and E. Tondello, *Thin Solid Films*, 2003, **442**, 48-52.
226. S. C. Ray, *Sol. Energ. Mat. Sol. C.*, 2001, **68**, 307-312.
227. C.-T. Hsieh, J.-M. Chen, H.-H. Lin and H.-C. Shih, *Appl. Phys. Lett.*, 2003, **82**, 3316-3318.
228. Y.-k. Su, C.-m. Shen, H.-t. Yang, H.-l. Li and H.-j. Gao, *T. Nonferr. Metal Soc.*, 2007, **17**, 783-786.
229. X. Hong, G. Wang, W. Zhu, X. Shen and Y. Wang, *J. Phys. Chem. C*, 2009, **113**, 14172-14175.
230. H. Wu, D. Lin and W. Pan, *Appl. Phys. Lett.*, 2006, **89**, 133125-133123.
231. S. M. Sze and K. K. Ng, *Physics of Semiconductor Devices*, John Wiley and Sons, New Jersey, 2007.
232. R. P. Wijesundera, *Semicond. Sci. Tech.*, 2010, **25**.
233. Y. Hames and S. E. San, *Sol. Energy*, 2004, **77**, 291-294.
234. D. Li, C.-J. Chien, S. Deora, P.-C. Chang, E. Moulin and J. G. Lu, *Chem. Phys. Lett.*, 2011, **501**, 446-450.
235. A. R. Zainun, S. Tomoya, U. Mohd Noor, M. Rusop and I. Masaya, *Mater. Lett.*, 2012, **66**, 254-256.
236. M. Wang, L. Sun, Z. Lin, J. Cai, K. Xie and C. Lin, *Energ. Environ. Sci.*, 2013, **6**, 1211-1220.
237. T. Minami, Y. Nishi and T. Miyata, *Appl. Phys. Express*, 2013, **6**.
238. K. P. Musselman, A. Wisnet, D. C. Iza, H. C. Hesse, C. Scheu, J. L. MacManus-Driscoll and L. Schmidt-Mende, *Adv. Mater.*, 2010, **22**, E254-E285.
239. T. Minami, Y. Nishi, T. Miyata and J. Nomoto, *Appl. Phys. Express*, 2011, **4**, 62301.
240. P. Raksa, S. Nilphai, A. Gardchareon and S. Choopun, *Thin Solid Films*, 2009, **517**, 4741-4744.
241. M. H. Kim and Y. U. Kwon, *J. Phys. Chem. C*, 2011, **115**, 23120-23125.
242. R. Sahay, J. Sundaramurthy, P. S. Kumar, V. Thavasi, S. G. Mhaisalkar and S. Ramakrishna, *J. Solid State Chem.*, 2012, **186**, 261-267.
243. S. Anandan, X. G. Wen and S. H. Yang, *Mater. Chem. Phys.*, 2005, **93**, 35-40.
244. H.-S. Koo, D.-T. Wang, Y.-K. Yu, S.-H. Ho, J.-Y. Jhang, M. Chen and M.-F. Tai, *Jpn. J. Appl. Phys.*, 2012, **51**.
245. G. B. Murdoch, M. Greiner, M. G. Helander, Z. B. Wang and Z. H. Lu, *Appl. Phys. Lett.*, 2008, **93**.
246. W. P. Hu, K. Manabe, T. Furukawa and M. Matsumura, *Appl. Phys. Lett.*, 2002, **80**, 2640-2641.

247. T. Satoh and H. Fujikawa, *Jpn. J. Appl. Phys. 1*, 2007, **46**, 1640-1642.
248. Z. Zheng, B. Huang, Z. Wang, M. Guo, X. Qin, X. Zhang, P. Wang and Y. Dai, *J. Phys. Chem. C*, 2009, **113**, 14448-14453.
249. M. Vaseem, A. Umar, Y. B. Hahn, D. H. Kim, K. S. Lee, J. S. Jang and J. S. Lee, *Catal. Commun.*, 2008, **10**, 11-16.
250. S. P. Meshram, P. V. Adhyapak, U. P. Mulik and D. P. Amalnerkar, *Chem. Eng. J.*, 2012, **204–206**, 158-168.
251. H. Xu, G. Zhu, D. Zheng, C. Xi, X. Xu and X. Shen, *J. Colloid Interf. Sci.*, 2012, **383**, 75-81.
252. J. Liu, J. Jin, Z. Deng, S.-Z. Huang, Z.-Y. Hu, L. Wang, C. Wang, L.-H. Chen, Y. Li, G. Van Tendeloo and B.-L. Su, *J. Colloid Interf. Sci.*, 2012, **384**, 1-9.
253. M.-h. Yao, Y.-g. Tang, L. Zhang, H.-h. Yang and J.-h. Yan, *T. Nonferr. Metal Soc.*, 2010, **20**, 1944-1949.
254. M. Hara, T. Kondo, M. Komoda, S. Ikeda, K. Shinohara, A. Tanaka, J. N. Kondo and K. Domen, *Chem. Commun.*, 1998, 357-358.
255. P. E. de Jongh, D. Vanmaekelbergh and J. J. Kelly, *Chem. Commun.*, 1999, 1069-1070.
256. G. K. Mor, O. K. Varghese, R. H. T. Wilke, S. Sharma, K. Shankar, T. J. Latempa, K. S. Choi and C. A. Grimes, *Nano Lett.*, 2008, **8**, 1906-1911.
257. W. Siripala, A. Ivanovskaya, T. F. Jaramillo, S. H. Baeck and E. W. McFarland, *Sol. Energ. Mat. Sol. C.*, 2003, **77**, 229-237.
258. M. Ni, M. K. H. Leung, D. Y. C. Leung and K. Sumathy, *Renew. Sust. Energ. Rev.*, 2007, **11**, 401-425.
259. N. Strataki, V. Bekiari, D. I. Kondarides and P. Lianos, *Appl. Catal. B-Environ.*, 2007, **77**, 184-189.
260. J. Bandara, C. P. K. Udawatta and C. S. K. Rajapakse, *Photochem. Photobio. S.*, 2005, **4**, 857-861.
261. S. Song, J. Tu, L. Xu, X. Xu, Z. He, J. Qiu, J. Ni and J. Chen, *Chemosphere*, 2008, **73**, 1401-1406.
262. H. Yang, J. Yan, Z. Lu, X. Cheng and Y. Tang, *J. Alloy Compd.*, 2009, **476**, 715-719.
263. A. Azam, A. S. Ahmed, M. Oves, M. S. Khan and A. Memic, *Int. J. Nanomed.*, 2012, **7**, 3527-3535.
264. N. Ekthammathat, T. Thongtem and S. Thongtem, *Appl. Surf. Sci.*, 2013, **277**, 211-217.
265. M. S. Hassan, T. Amna, O. B. Yang, M. H. El-Newehy, S. S. Al-Deyab and M.-S. Khil, *Colloid Surface B*, 2012, **97**, 201-206.
266. I. Perelshtein, G. Applerot, N. Perkas, E. Wehrschuetz-Sigl, A. Hasmann, G. Guebitz and A. Gedanken, *Surf. Coat. Tech.*, 2009, **204**, 54-57.
267. G. Ren, D. Hu, E. W. C. Cheng, M. A. Vargas-Reus, P. Reip and R. P. Allaker, *Int. J. Antimicrob. Ag.*, 2009, **33**, 587-590.
268. M. Paschoalino, N. C. Guedes, W. Jardim, E. Mieluarski, J. A. Mielczarski, P. Bowen and J. Kiwi, *J. Photoch. Photobio. A*, 2008, **199**, 105-111.
269. O. Akhavan and E. Ghaderi, *Journal of Materials Chemistry*, 2011, **21**, 12935-12940.
270. P. Demchick and A. L. Koch, *J. Bacteriol.*, 1996, **178**, 768-773.
271. B. Wang, X.-L. Wu, C.-Y. Shu, Y.-G. Guo and C.-R. Wang, *J. Mater. Chem.*, 2010, **20**, 10661-10664.
272. J. Y. Xiang, J. P. Tu, L. Zhang, Y. Zhou, X. L. Wang and S. J. Shi, *J. Power Sources*, 2010, **195**, 313-319.
273. L. Ji, Z. Lin, M. Alcoutlabi and X. Zhang, *Energ. Environ. Sci.*, 2011, **4**, 2682-2699.
274. Y. J. Mai, X. L. Wang, J. Y. Xiang, Y. Q. Qiao, D. Zhang, C. D. Gu and J. P. Tu, *Electrochim. Acta*, 2011, **56**, 2306-2311.
275. J. Zhou, L. Ma, H. Song, B. Wu and X. Chen, *Electrochem. Commun.*, 2011, **13**, 1357-1360.
276. J. C. Park, J. Kim, H. Kwon and H. Song, *Adv. Mater.*, 2009, **21**, 803-+.
277. W. Wei, Z. Wang, Z. Liu, Y. Liu, L. He, D. Chen, A. Umar, L. Guo and J. Li, *J. Power Sources*, 2013, **238**, 376-387.
278. R. Neskovska, M. Ristova, J. Velevska and M. Ristov, *Thin Solid Films*, 2007, **515**, 4717-4721.
279. M. Ristova, R. Neskovska and V. Mirčeski, *Sol. Energ. Mater. Sol. C.*, 2007, **91**, 1361-1365.
280. T. J. Richardson, J. L. Slack and M. D. Rubin, *Electrochim. Acta*, 2001, **46**, 2281-2284.
281. O. Akhavan, H. Tohidi and A. Z. Moshfegh, *Thin Solid Films*, 2009, **517**, 6700-6706.
282. J. Z. Ou, S. Balendhran, M. R. Field, D. G. McCulloch, A. S. Zoolfakar, R. A. Rani, S. Zhuiykov, A. P. O'Mullane and K. Kalantar-zadeh, *Nanoscale*, 2012, **4**, 5980-5988.
283. T. Y. Zhai, X. S. Fang, M. Y. Liao, X. J. Xu, H. B. Zeng, B. Yoshio and D. Golberg, *Sensors*, 2009, **9**, 6504-6529.
284. S. B. Wang, C. H. Hsiao, S. J. Chang, K. T. Lam, K. H. Wen, S. C. Hung, S. J. Young and B. R. Huang, *Sens. Actuator A Phys.*, 2011, **171**, 207-211.
285. S. Sahoo, S. Husale, B. Colwill, T.-M. Lu, S. Nayak and P. M. Ajayan, *ACS Nano*, 2009, **3**, 3935-3944.
286. B. J. Hansen, N. Kouklin, G. Lu, I. K. Lin, J. Chen and X. Zhang, *J. Phys. Chem. C*, 2010, **114**, 2440-2447.
287. S. Manna, K. Das and S. K. De, *ACS Appl. Mater. Inter.*, 2010, **2**, 1536-1542.
288. J. Xu, J.-L. Sun, J. Wei and J. Xu, *Appl. Phys. Lett.*, 2012, **100**.
289. A. Tricoli, M. Righettoni and A. Teleki, *Angew. Chem. Int. Edit.*, 2010, **49**, 7632-7659.
290. H. Kim, C. Jin, S. Park, S. Kim and C. Lee, *Sens. Actuator B-Chem.*, 2012, **161**, 594-599.
291. X. Gou, G. Wang, J. Yang, J. Park and D. Wexler, *J. Mater. Chem.*, 2008, **18**, 965-969.
292. G. X. Zhu, H. Xu, Y. Y. Xiao, Y. J. Liu, A. H. Yuan and X. P. Shen, *ACS Appl. Mater. Interfaces*, 2012, **4**, 744-751.
293. M. Ando, T. Kobayashi and M. Haruta, *Catal. Today*, 1997, **36**, 135-141.
294. X.-W. Liu, F.-Y. Wang, F. Zhen and J.-R. Huang, *RSC Advances*, 2012, **2**, 7647-7651.
295. H. T. Hsueh, S. J. Chang, F. Y. Hung, W. Y. Weng, C. L. Hsu, T. J. Hsueh, S. S. Lin and B. T. Dai, *J. Electrochem. Soc.*, 2011, **158**, J106-J109.
296. Y. Zhang, X. He, J. Li, H. Zhang and X. Gao, *Sens. Actuator B Chem.*, 2007, **128**, 293-298.
297. H. G. Zhang, Q. S. Zhu, Y. Zhang, Y. Wang, L. Zhao and B. Yu, *Adv. Funct. Mater.*, 2007, **17**, 2766-2771.
298. D. Barreca, E. Comini, A. Gasparotto, C. Maccato, C. Sada, G. Sberveglieri and E. Tondello, *Sensor Actuat. B-Chem.*, 2009, **141**, 270-275.
299. L. Liao, Z. Zhang, B. Yan, Z. Zheng, Q. L. Bao, T. Wu, C. M. Li, Z. X. Shen, J. X. Zhang, H. Gong, J. C. Li and T. Yu, *Nanotechnology*, 2009, **20**.
300. Y.-S. Kim, I.-S. Hwang, S.-J. Kim, C.-Y. Lee and J.-H. Lee, *Sens. Actuator B-Chem.*, 2008, **135**, 298-303.
301. F. Zhang, A. W. Zhu, Y. P. Luo, Y. Tian, J. H. Yang and Y. Qin, *J. Phys. Chem. C*, 2010, **114**, 19214-19219.
302. T. Asefa, C. T. Duncan and K. K. Sharma, *Analyst*, 2009, **134**, 1980-1990.
303. S. Park, H. Boo and T. D. Chung, *Anal. Chim. Acta*, 2006, **556**, 46-57.
304. Z. J. Zhuang, X. D. Su, H. Y. Yuan, Q. Sun, D. Xiao and M. M. F. Choi, *Analyst*, 2008, **133**, 126-132.
305. L. Zhang, H. Li, Y. H. Ni, J. Li, K. M. Liao and G. C. Zhao, *Electrochem. Commun.*, 2009, **11**, 812-815.
306. C. Batchelor-McAuley, Y. Du, G. G. Wildgoose and R. G. Compton, *Sens. Actuators B: Chem.*, 2008, **135**, 230-235.
307. C. Batchelor-McAuley, G. G. Wildgoose, R. G. Compton, L. Shao and M. L. H. Green, *Sens. Actuators B: Chem.*, 2008, **132**, 356-360.
308. A. H. Battez, R. Gonzalez, J. L. Viesca, J. E. Fernandez, J. M. D. Fernandez, A. Machado, R. Chou and J. Riba, *Wear*, 2008, **265**, 422-428.
309. T. Oishi, M. Goto, A. Kasahara and M. Tosa, *Surf. Interface Anal.*, 2004, **36**, 1259-1261.
310. M. A. Kedzierski, *Int. J. Refrig.*, 2012, **35**, 1997-2002.
311. S.-s. Bi, L. Shi and L.-l. Zhang, *Appl. Therm. Eng.*, 2008, **28**, 1834-1843.
312. S. Lee, S. U. S. Choi, S. Li and J. A. Eastman, *J. Heat Trans-T Asme*, 1999, **121**, 280-289.
313. C. T. Hsieh, J. M. Chen, H. H. Lin and H. C. Shih, *Appl. Phys. Lett.*, 2003, **83**, 3383-3385.

314. Y. W. Zhu, T. Yu, F. C. Cheong, X. J. Xui, C. T. Lim, V. B. C. Tan, J. T. L. Thong and C. H. Sow, *Nanotechnology*, 2005, **16**, 88-92.
315. Y. Wang, S. C. Li, H. Shi and K. Yu, *Nanoscale*, 2012, **4**, 7817-7824.
316. R. C. Wang and C. H. Li, *Cryst. Growth Des.*, 2009, **9**, 2229-2234.
317. Y. Wang, K. Yu, H. H. Yin, C. Q. Song, Z. L. Zhang, S. C. Li, H. Shi, Q. F. Zhang, B. Zhao, Y. F. Zhang and Z. Q. Zhu, *J. Phys. D Appl. Phys.*, 2013, **46**.
318. S. Tanaka, Y. Sawai and A. Chiba, *J. Eur, Ceram. Soc.*, 2004, **24**, 289-293.
319. K. Krishnamoorthy and S.-J. Kim, *Mater. Res. Bull.*, 2013, **48**, 3136-3139.
320. D. P. Dubal, G. S. Gund, C. D. Lokhande and R. Holze, *Mater. Res. Bull.*, 2013, **48**, 923-928.
321. B. Singh, B. R. Mehta, D. Varandani, A. V. Savu and J. Brugger, *Nanotechnology*, 2012, **23**.
322. A. Chen, S. Haddad, Y. C. Wu, Z. Lan, T. N. Fang and S. Kaza, *Appl. Phys. Lett.*, 2007, **91**.
323. W.-Y. Yang, W.-G. Kim and S.-W. Rhee, *Thin Solid Films*, 2008, **517**, 967-971.
324. I. Najdovski, P. Selvakannan, S. K. Bhargava and A. P. O'Mullane, *Nanoscale*, 2012, **4**, 6298-6306.
325. J. B. Reitz and E. I. Solomon, *J. Am. Chem. Soc.*, 1998, **120**, 11467-11478.
326. S. Song, R. Rao, H. Yang and A. Zhang, *J. Phys. Chem. C*, 2010, **114**, 13998-14003.
327. Y. Xu, H. Wang, Y. Yu, L. Tian, W. Zhao and B. Zhang, *J. Phys. Chem. C*, 2011, **115**, 15288-15296.
328. R. Prucek, L. Kvitek, A. Panacek, L. Vancurova, J. Soukupova, D. Jancik and R. Zboril, *J. Mater. Chem.*, 2009, **19**, 8463-8469.
329. S. Zhuiykov, E. Kats, D. Marney and K. Kalantar-zadeh, *Prog. Org. Coat.*, 2011, **70**, 67-73.
330. S. Zhuiykov and K. Kalantar-zadeh, *Electrochim. Acta*, 2012, **73**, 105-111.
331. S. Zhuiykov, D. Marney, E. Kats and K. Kalantar-Zadeh, *Sens. Actuator B Chem.*, 2011, **153**, 312-320.
332. E. Fortunato, V. Figueiredo, P. Barquinha, E. Elamurugu, R. Barros, G. Goncalves, S.-H. K. Park, C.-S. Hwang and R. Martins, *Appl. Phys. Lett.*, 2010, **96**.
333. X. Zou, G. Fang, L. Yuan, M. Li, W. Guan and X. Zhao, *IEEE Electrn Device L.*, 2010, **31**, 827-829.

Table 1. Crystallographic properties of CuO, Cu_2O and Cu_4O_3 [1-6]

	CuO	Cu_2O	Cu_4O_3
Lattice	Monoclinic a = 4.6837 Å b = 3.4226 Å c = 5.1288 Å β = 99.54° α = γ = 90º	Cubic a = 4.2696 Å	Tetragonal a = 5.837 Å b = 9.932 Å
Shortest distance			
Interatomic distances Cu — O	1.95 Å	1.84 Å	1.87 Å
Interatomic distances O — O	2.62 Å	3.68 Å	2.56 Å
Interatomic distances Cu — Cu	2.90 Å	3.01 Å	2.92 Å
Formula weight	79.57	143.14	302.18
Density	6.52 gcm^{-3}	5.75 gcm^{-3}	5.93 gcm^{-3}
Melting point	1201 ºC	1235 ºC	400 ºC
Cell volume	81.08 $Å^3$	77.833 × 10^{-24} cm^{-3}	338 $Å^3$

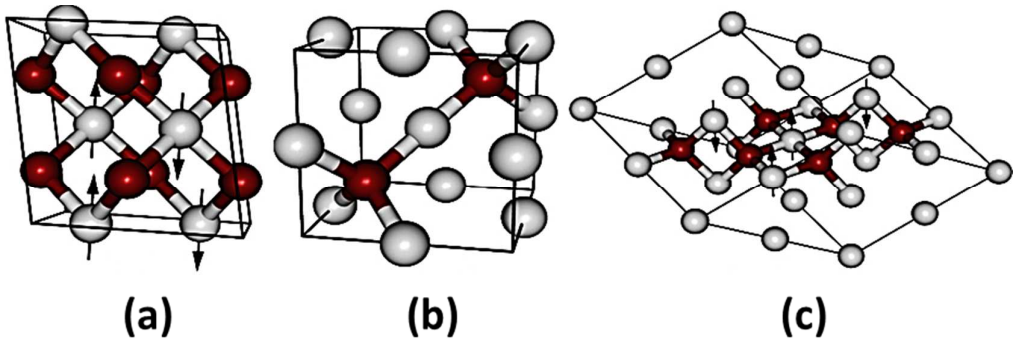

Figure 1. Monoclinic, cubic and tetragonal crystal structure of the copper oxide compounds (a) CuO, (b) Cu_2O and (c) Cu_4O_3 (gray and red spheres represent copper and oxygen atoms, respectively). For the antiferromagnetic CuO and Cu_4O_3 the arrows on the copper ions indicate the orientation of local magnetic moments. Reprinted figure with permission from (M. Heinemann, B. Eifert and C. Heiliger, *Phys. Rev. B*, 2013, 87) copyright (2013) by the American Physical Society.

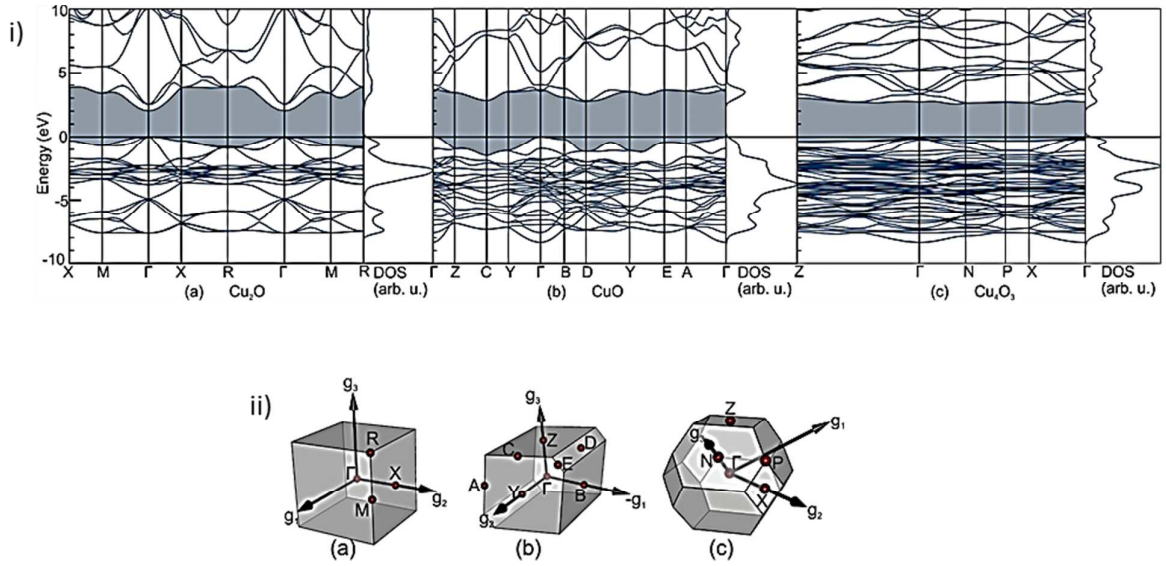

Figure 2. (i) Electronic band structure and density of states from hybrid functional DFT calculations and (ii) Brillouin zones with special high symmetry *k* points of the three copper oxide compounds to: (a) Cu_2O, (b) CuO and (c) Cu_4O_3. Reprinted figure with permission from (M. Heinemann, B. Eifert and C. Heiliger, *Phys. Rev. B*, 2013, 87) copyright (2013) by the American Physical Society.

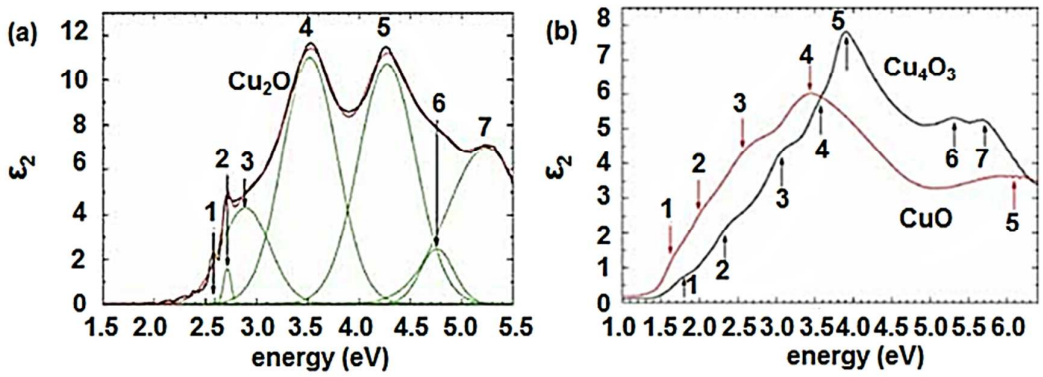

Figure 3. Gaussian fit to the imaginary part of the dielectric ε_2 for (a) Cu_2O, (b) CuO and Cu_4O_3. Reprinted with permission from (B. K. Meyer, A. Polity, D. Reppin, M. Becker, P. Hering, P. J. Klar, T. Sander, C. Reindl, J. Benz, M. Eickhoff, C. Heiliger, M. Heinemann, J. Blaesing, A. Krost, S. Shokovets, C. Mueller and C. Ronning, *Phys. Status Solidi B*, 2012, 249, 1487-1509) copyright (2012) by WILEY-VCH Verlag GmbH & Co. KGaA, Weinheim.

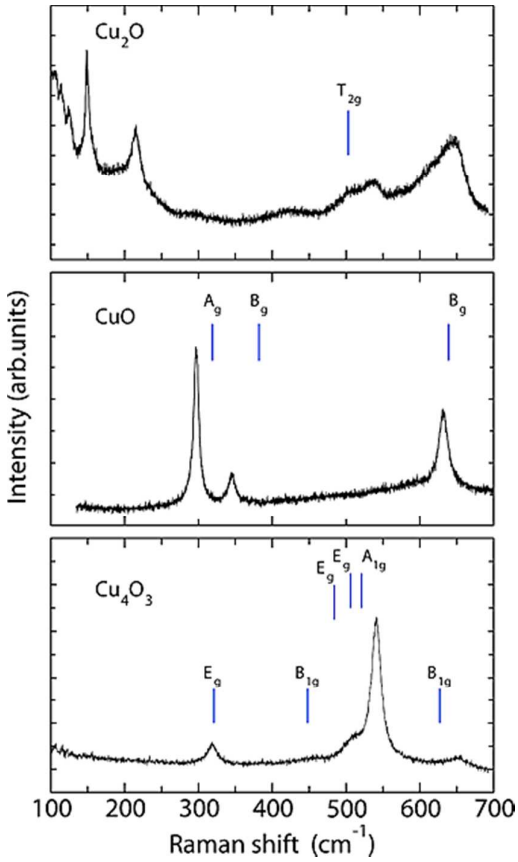

Figure 4. Experimental Raman spectra of Cu_2O, CuO and Cu_4O_3. The calculated frequencies of Raman active vibrational modes are indicated by vertical bars. Reprinted with permission from (L. Debbichi, M. C. M. de Lucas, J. F. Pierson and P. Kruger, *J. Phys. Chem. C*, 2012, 116, 10232-10237) copyright (2012) American Chemical Society.

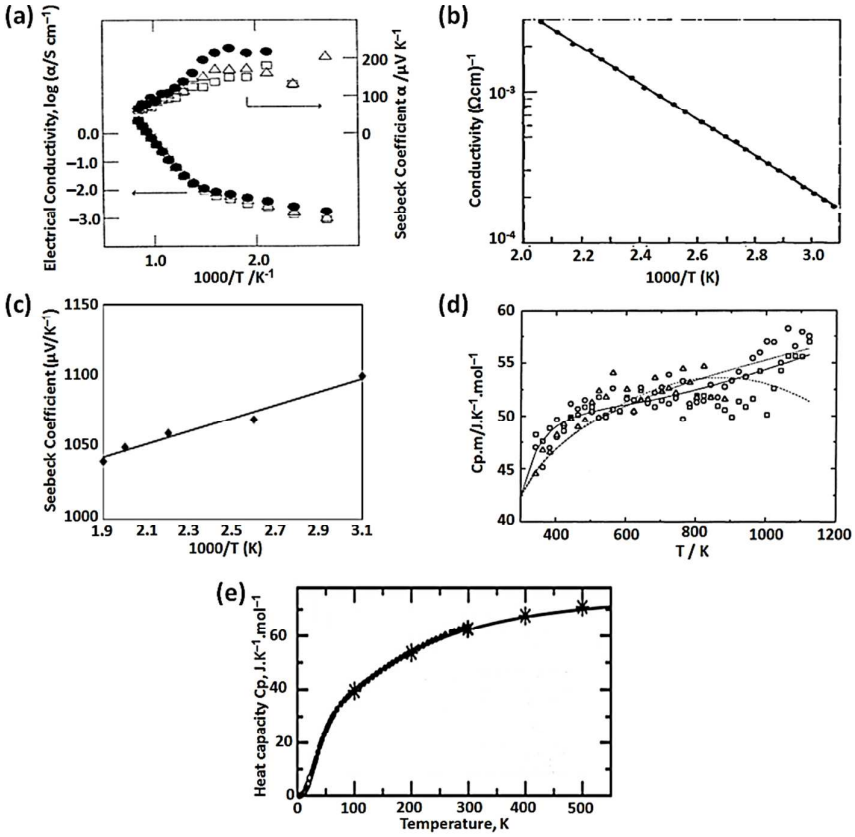

Figure 5. (a) Temperature dependence for electrical conductivity and Seebeck coefficient of CuO in oxygen (●), in air (Δ) and in 3% O_2–Ar (□), (b) Electrical conductivity of Cu_2O single crystal *vs* 1/*T*, (c) Seebeck coefficient of Cu_2O single crystal *vs* 1/*T*, calculated and experimental heat capacities, C_p of (d) CuO: (□ Δ ○) Ref 89, (· · ·) Ref 90, (---) Ref 91, and (e) Cu_2O: (—) Ref 88, (○) Ref 92 (●) Ref 93. Reprinted with permission from (a) (S. Suda, S. Fujitsu, K. Koumoto and H. Yanagida, *Jpn. J. Appl. Phys. 1*, 1992, 31, 2488-2491) copyright (1992) by The Japan Society of Applied Physics, (b and c) Reprinted from *J. Phys. Chem. Solids,* 30, A. P. Young and C. M. Schwartz, 249-25, copyright (1969) with permission from Elsevier, (d) Reprinted from *Thermochim. Acta,* 348, J. Leitner, D. Sedmidubský, B. Doušová, A. Strejc and M. Nevřiva 49-51, copyright (2000) with permission from Elsevier, (e) (P. A. Korzhavyi, I. L. Soroka, E. I. Isaev, C. Lilja and B. Johansson, *P. Natl. Acad. Sci. USA*, 2012, 109, 686-689) copyright (2012) National Academy of Science, USA.

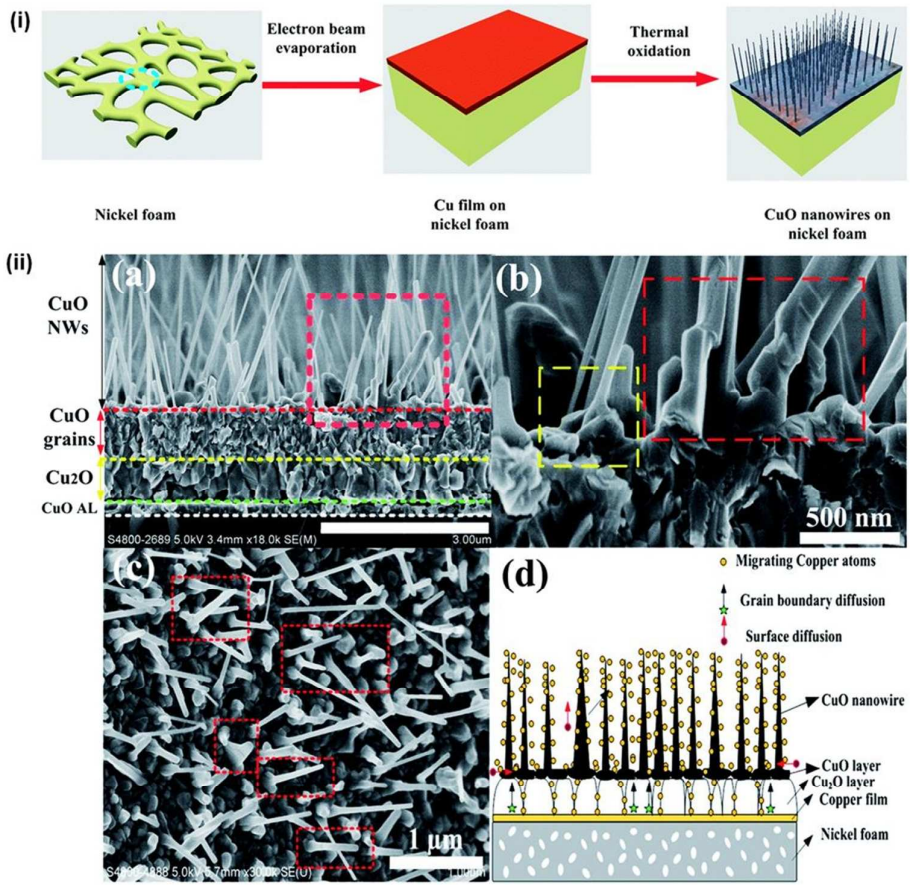

Figure 6. (i) Schematic illustration of the synthesis process for CuO nanowires on nickel foam. (ii) (a) cross-sectional view of CuO nanowires synthesized on the CuO adhesion layer (AL)/Si substrate, (b) magnified view from the nanowire root region marked by the red dashed square, (c) top-view of CuO nanowires synthesized on Ni foam and (d) illustration of the mechanism for CuO nanowires growth. Reproduced from Ref. 148 with permission from The Royal Society of Chemistry.

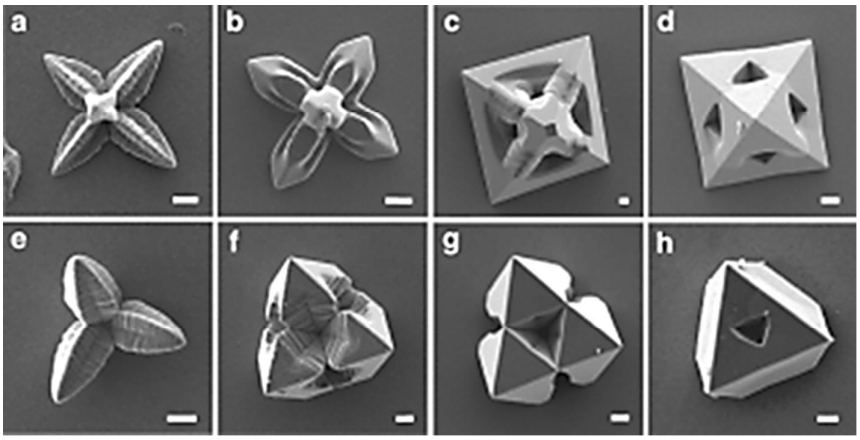

Figure 7. SEM images of deposited octahedral Cu_2O crystals that display systematically varying degrees of branching with (100) planes parallel to the substrate (a–d) and with (111) planes parallel to the substrate (e–h). These crystals were obtained at a constant temperature (60 °C) and concentration of Cu^{2+} (0.02 M) and by applying a deposition conditions of 0.10 mA $cm^{-2} \leq I \leq$ 0.12 mA cm^{-2} and 0.08 V $\leq E \leq$ 0.12 V. All figures have scale bars of 1 μm. Reprinted with permission from (M. J. Siegfried and K. S. Choi, *Angew. Chem. Int. Edit.*, 2005, 44, 3218-3223) copyright (2012) by WILEY-VCH Verlag GmbH & Co. KGaA, Weinheim.

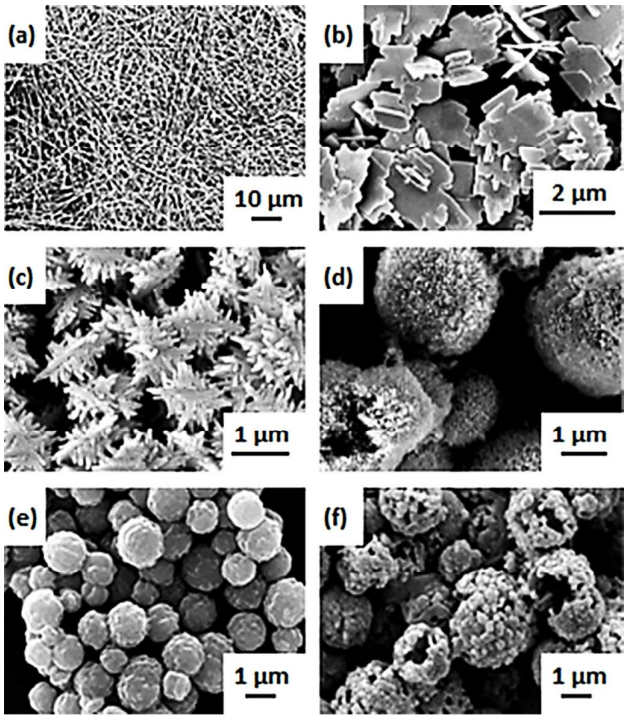

Figure 8. SEM images of various morphologies *via* hydrothermally/solvothermally synthesized of (a) Cu_2O nanowires synthesized at 180 °C in Copper (II) acetate aqueous solution with pyrrole, (b) CuO flake–like synthesized at 200 °C in Copper (II) sulphate aqueous, (c) CuO/Cu_2O dendrite–like synthesized at 200 °C in Copper (II) sulphate aqueous with 10 ml ethylene glycol (EG), (d) CuO/Cu_2O flower–like synthesized at 200 °C in Copper (II) sulphate aqueous with 20 ml EG, and CuO/Cu_2O composite hollow microspheres obtained in a Copper (II) acetate aqueous solution at 200 °C for (e) 1 hour and (f) 5 hours. Reprinted with permission from (a) (Y. W. Tan, X. Y. Xue, Q. Peng, H. Zhao, T. H. Wang and Y. D. Li, *Nano Lett.*, 2007, **7**, 3723-3728) copyright (2007) American Chemical Society, (b,c,d) (S. Z. Li, H. Zhang, Y. J. Ji and D. R. Yang, *Nanotechnology*, 2004, 15, 1428-1432) copyright (2004) by IOP Publishing Ltd, (e,f) (H. Yu, J. Yu, S. Liu and S. Mann, *Chem. Mater.*, 2007, 19, 4327-4334) copyright (2007) American Chemical Society.

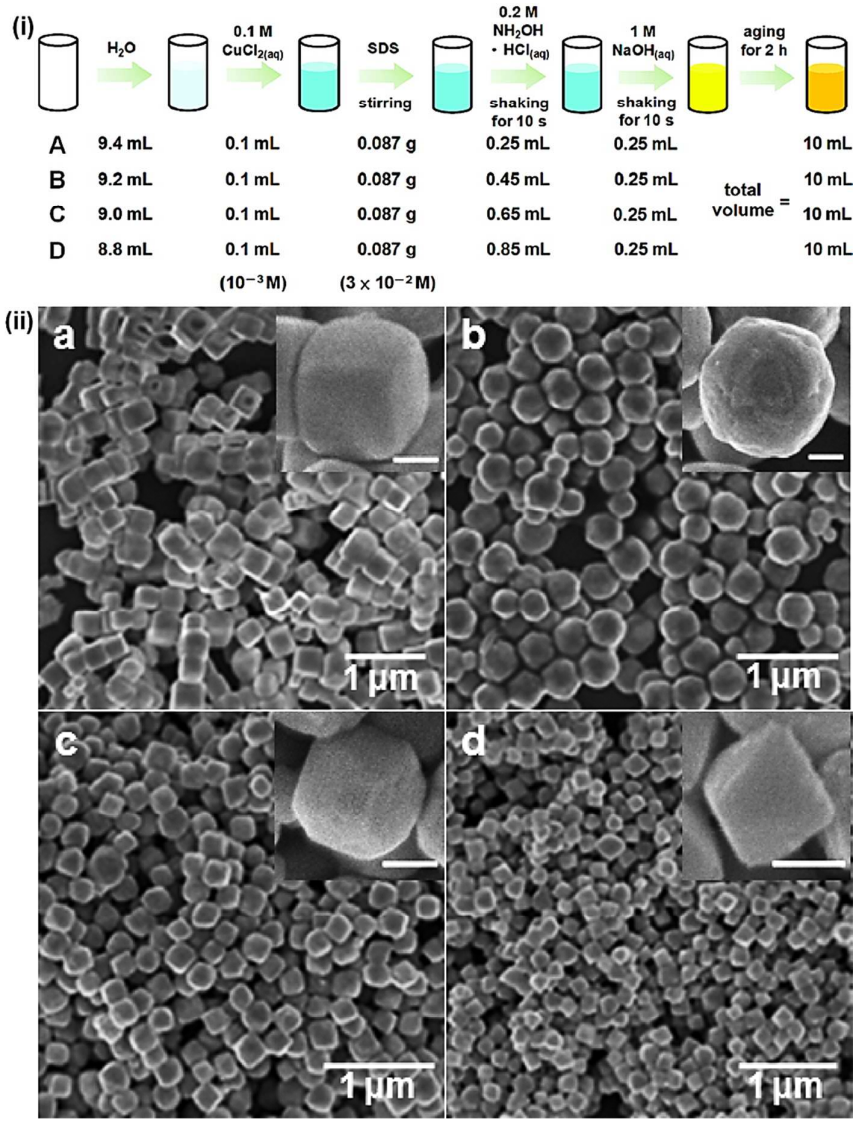

Figure 9. (i) Schematic illustration of the procedure used for growing Cu_2O nanocrystals of different shapes. (ii) (a-d) Respective SEM images of the Cu_2O nanocrystals synthesized in sample containers A, B, C and D with increasing amounts of NH_2OH•HC added to the solutions. The particle morphologies are (a) truncated cubic, (b) cuboctadheral, (c) truncated octahedral and (d) octahedral in shape. Insets show the enlarged views of individual nanocrsytals. The scale bars in the insets are 100 nm. Reprinted with permission from (C.-H. Kuo and M. H. Huang, *J. Phys. Chem. C*, 2008, 112, 18355-18360) copyright (2007) American Chemical Society.

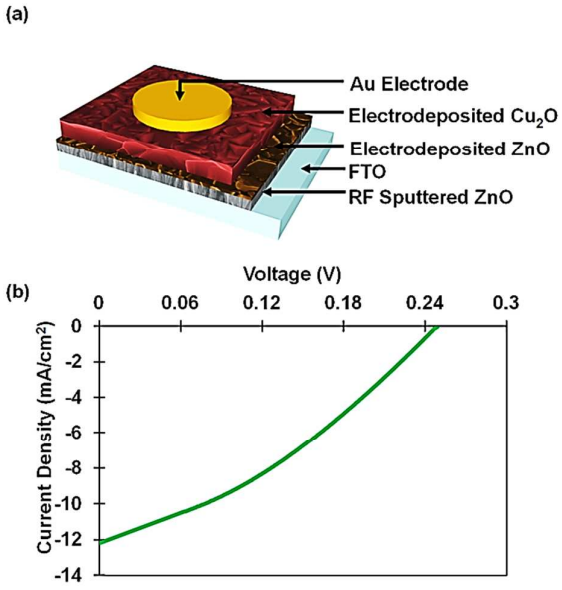

Figure 10. (a) 3D schematic of the electrodeposited ZnO–Cu_2O heterojunction solar cells, (b) *J*–*V* characteristic curves of ZnO–Cu_2O heterojunction solar cells. Reproduced from Ref. 173 with permission from The Royal Society of Chemistry.

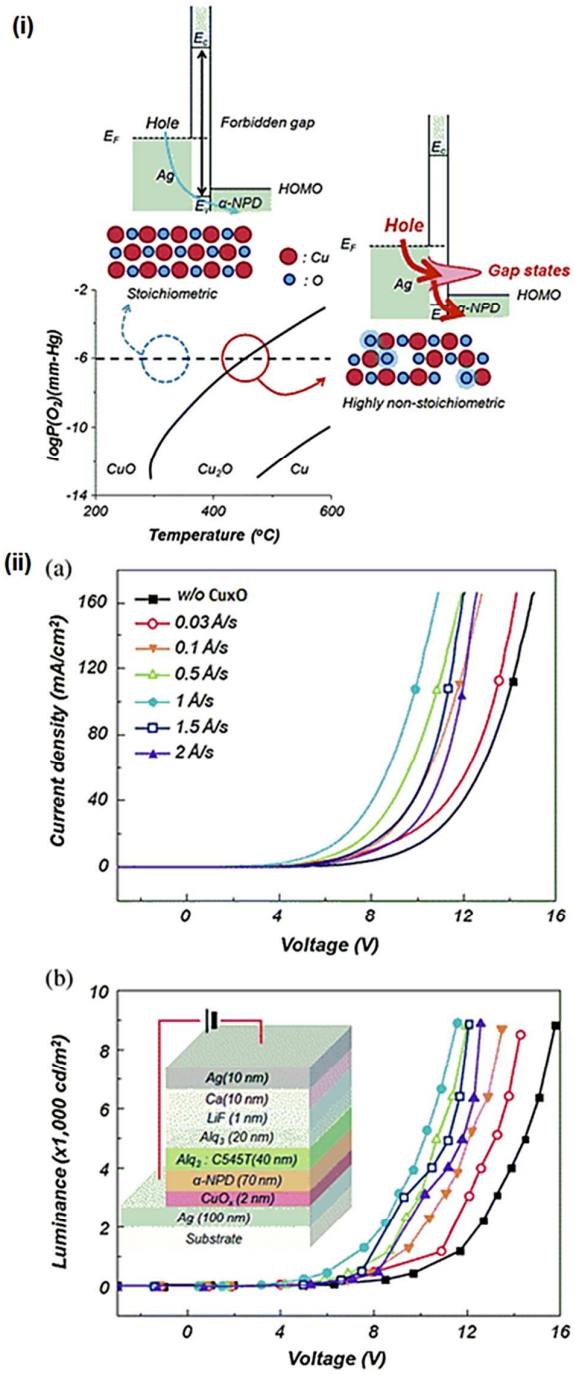

Figure 11. (i) Phase diagram of a copper-oxygen binary system and schematic diagram of electronic states and film structure of stoichiometric and non-stoichiometric Cu_xO, (ii) (a) current-density voltage (*J*–*V*) and (b) luminance-voltage (*L*–*V*) characteristics of OLED with Cu_xO HIL deposited at

different rates. Inset: schematic diagram of OLEDs. Reproduced from Ref. 134 with permission from The Royal Society of Chemistry.

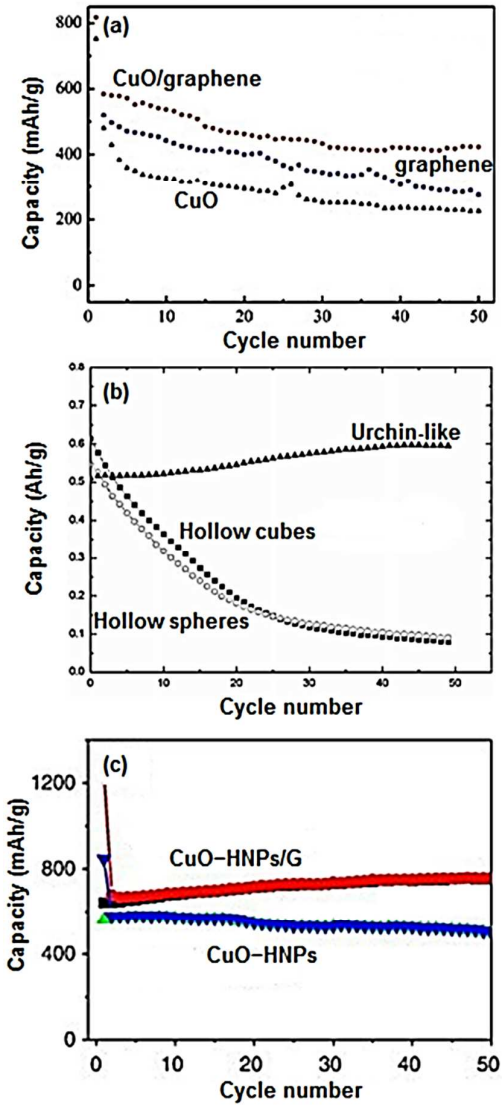

Figure 12. Cycling profile of (a) bare CuO, graphene and CuO/graphene electrode at current density of 67 mAg^{-1}, (b) CuO nanoparticles with three types morphologies (urchin−like, hollow cubes and hollow spheres) at a current density of 150 mAg^{-1}, (c) CuO hollow nanoparticles/graphene (CuO−HNPs/G) and CuO hollow nanoparticles (CuO−HNPs) at 50 mAg^{-1}. (a) Reprinted from *Electrochim. Acta,* 56, Y. J. Mai, X. L. Wang, J. Y. Xiang, Y. Q. Qiao, D. Zhang, C. D. Gu and J. P. Tu, 2306-2311, copyright (2011) with permission from Elsevier, (b) Reprinted with permission from (J. C. Park, J. Kim, H. Kwon and H. Song, *Adv. Mater.*, 2009, 21, 803) copyright (2009) by WILEY-VCH Verlag

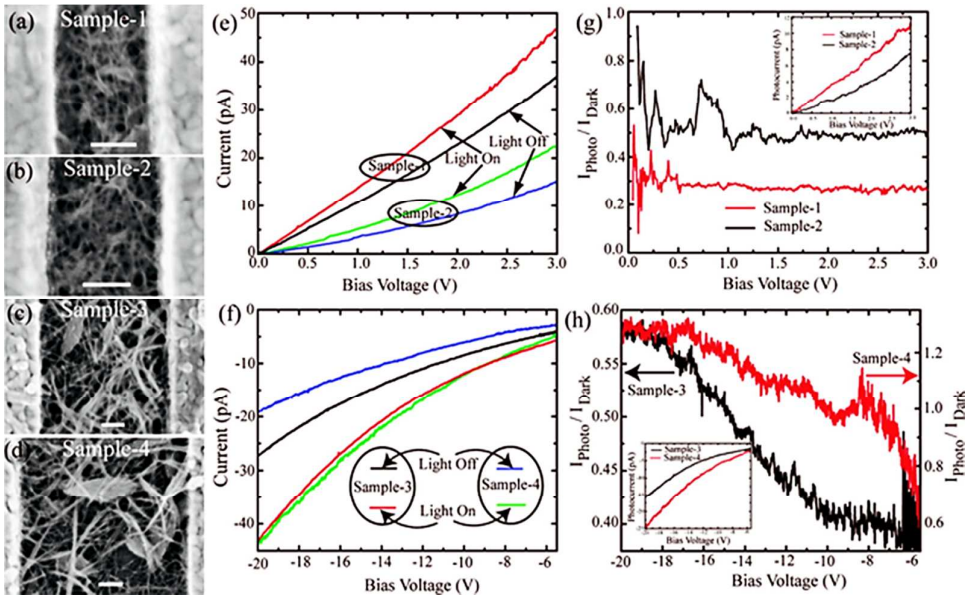

Figure 13. (a−d) SEM micrographs of Cu_2O nanowire base devices having electrode spacings of 210, 260, 580, and 720 nm, respectively. The electrodes are 3.2 µm wide for all of the devices. The scale bars are 100 nm. The current−voltage (*I*−*V*) measurements are carried out at dark and under illumination conditions for all four samples. Depending on the interelectrode spacing, the samples are categorized into two sets, set I: sample-1 and sample-2; set II: sample-3 and sample-4. (e,f) *I*−*V* characteristics of set I and set II, respectively. (g,h) Plot of the ratio of photocurrent (*I*photo) to the dark current (*I*dark) *vs* bias voltage for set I and set II, respectively. Insets of (g) and (h) represent the photocurrent as a function of bias for set I and set II, respectively. Reprinted with permission from (S. Sahoo, S. Husale, B. Colwill, T.-M. Lu, S. Nayak and P. M. Ajayan, *ACS Nano*, 2009, 3, 3935-3944) copyright (2007) American Chemical Society.

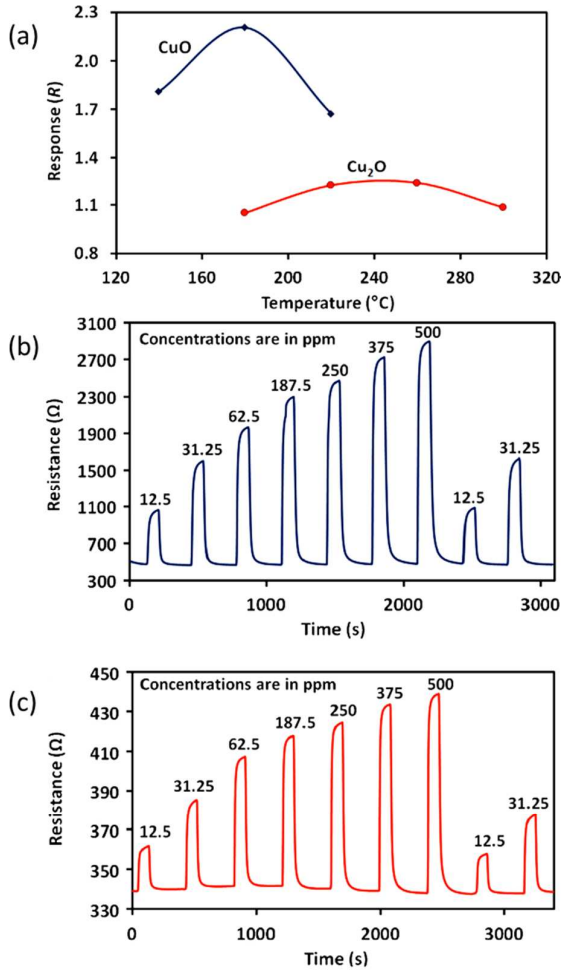

Figure 14. (a) Sensor response curves of the CuO and Cu_2O based sensors towards ethanol (12.5 ppm) at different operating temperatures, dynamic response of (b) CuO based sensors towards ethanol at the optimum operating temperature of 180 °C and (c) Cu_2O based sensors towards ethanol at the optimum operating temperature of 260 °C. Reprinted from *Sens. Actuator B Chem.*, 185, A. S. Zoolfakar, M. Z. Ahmad, R. A. Rani, J. Z. Ou, S. Balendhran, S. Zhuiykov, K. Latham, W. Wlodarski and K. Kalantar-zadeh, 620-627, copyright (2013) with permission Elsevier.

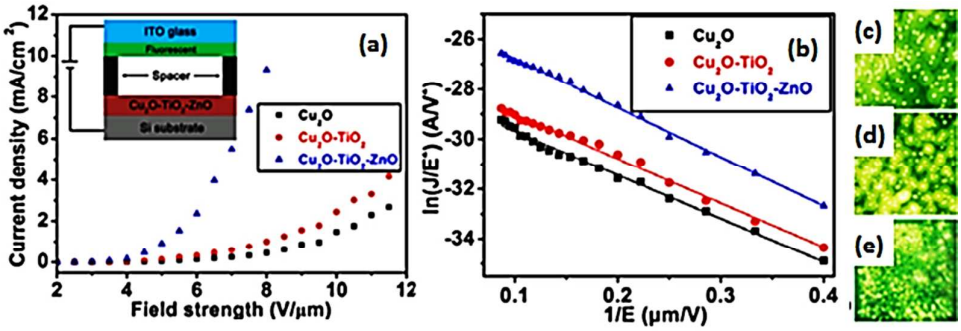

Figure 15. (a) Field emission *J*–*E* curves, (b) corresponding F–N plots of the samples. (c)–(e) Electron emission images of the pure Cu_2O nanopines, Cu_2O–TiO_2–ZnO composite samples, respectively. Reprinted with permission from (Y. Wang, K. Yu, H. H. Yin, C. Q. Song, Z. L. Zhang, S. C. Li, H. Shi, Q. F. Zhang, B. Zhao, Y. F. Zhang and Z. Q. Zhu, *J. Phys. D Appl. Phys.*, 2013, 46), copyright (2013) by IOP Publishing Ltd.